AD-A124 189 FACTORS INFLUENCING THERMOMECHANICAL FAILURE OF FACE SEALS II(U) THAYER SCHOOL OF ENGINEERING HANOVER N H F E KENNEDY ET AL. JAN 83 N00014-81-K-0090 1/1

UNCLASSIFIED F/G 11/1 NL

END
FILMED
DTIC

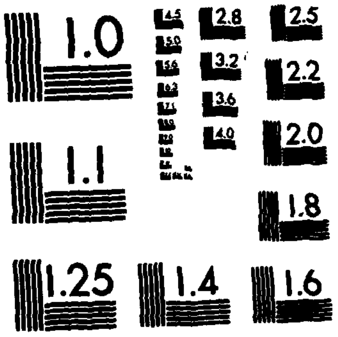
1.0
4.5
5.0
5.6
6.3
7.1
8.0
2.8
3.2
3.6
4.0
2.5
2.2
2.0
1.1
1.8
1.25
1.4
1.6

MICROCOPY RESOLUTION TEST CHART
NATIONAL BUREAU OF STANDARDS-1963-A

AD A124189

(12)

FACTORS INFLUENCING THERMOMECHANICAL FAILURE OF FACE SEALS II

by

Francis E. Kennedy, Jr.
Associate Professor of Engineering

and

[illegible] Grim and Roger P. Glovsky
Graduate Research Assistants

Interim Report #2
submitted to

Office of Naval Research
Contract No. N00014-81-K-0090
Period Covered: December 1, 1981 to November 30, 1982

January 1983

DTIC FILE COPY

DTIC
S ELECTE D
FEB 8 1983
B

DISTRIBUTION STATEMENT A
Approved for public release;
Distribution Unlimited

015

THAYER
SCHOOL
OF
ENGINEERING

1867

Unclassified

SECURITY CLASSIFICATION OF THIS PAGE (When Data Entered)

REPORT DOCUMENTATION PAGE

READ INSTRUCTIONS BEFORE COMPLETING FORM

1. REPORT NUMBER

2. GOVT ACCESSION NO. A124189

3. RECIPIENT'S CATALOG NUMBER

4. TITLE (and Subtitle)
FACTORS INFLUENCING THERMOMECHANICAL
FAILURE OF FACE SEALS II

5. TYPE OF REPORT & PERIOD COVERED
Interim Report #2
Dec 1, 1981 - Nov. 30, 1982

6. PERFORMING ORG. REPORT NUMBER

7. AUTHOR(s)
Francis E. Kennedy, Jr.
John N. Grim
Roger P. Glovsky

8. CONTRACT OR GRANT NUMBER(s)
N00014-81-K-0090

9. PERFORMING ORGANIZATION NAME AND ADDRESS
Thayer School of Engineering
Dartmouth College
Hanover, New Hampshire 03755

10. PROGRAM ELEMENT, PROJECT, TASK AREA & WORK UNIT NUMBERS

11. CONTROLLING OFFICE NAME AND ADDRESS
Engineering Science Directorate
Office of Naval Research
Arlington, Virginia 22217

12. REPORT DATE
January 1983

13. NUMBER OF PAGES
72

14. MONITORING AGENCY NAME & ADDRESS (if different from Controlling Office)

15. SECURITY CLASS. (of this report)
Unclassified

15a. DECLASSIFICATION/DOWNGRADING SCHEDULE

16. DISTRIBUTION STATEMENT (of this Report)

Approved for public release; distribution unlimited.

DTIC
ELECTE
FEB 8 1983
S D
B

17. DISTRIBUTION STATEMENT (of the abstract entered in Block 20, if different from Report)

18. SUPPLEMENTARY NOTES

19. KEY WORDS (Continue on reverse side if necessary and identify by block number)

Mechanical Seals, Face Seals, Seals, Thermoelastic Instability, Failure, Surface Temperature.

20. ABSTRACT (Continue on reverse side if necessary and identify by block number)

Analytical and experimental studies of factors affecting thermocracking and other modes of thermomechanical failure of mechanical face seals have continued for a second year.

In the experimental phase a unique contact probe/thermocouple has been built for studying characteristics of small patches of solid-to-solid contact at the sealing interface of mechanical face seals during seal operation. The probe was used to determine the number, size, location, and surface (pto)

DD FORM 1 JAN 73 1473 EDITION OF 1 NOV 65 IS OBSOLETE
S/N 0102-LF-014-6601

Unclassified

SECURITY CLASSIFICATION OF THIS PAGE (When Data Entered)

20. (continued)

temperature of contact patches over a range of seal velocities. Both dry and liquid-lubricated conditions were studied, and three different mating ring materials were tested. It was found that small, discrete contact patches are indeed present on the contact interface, that the patches tend to be stationary with respect to the metallic mating ring, whether that ring is stationary or rotating, and that the size and temperature of the contact spots is influenced by operating velocity and by the thermal, elastic, and wear properties of the seal materials.

The analytical phase of the study was focused on the prediction of surface temperatures at the patches of contact on the seal interface. A finite element surface temperature analysis program (THERMAP) was rewritten, documented, and proven out on a number of test problems. The program was used to study the influence of various operating and material parameters on the magnitude of the surface temperatures in the contact patches of face seals. It was found that the most promising approach to decreasing the surface temperatures would be to increase the thermal conductivity of the mating ring and primary ring materials. A decrease in seal velocity (by a decrease in diameter) and improved cooling of the seal faces would also serve to decrease surface temperatures. It was also found that numerical oscillations can develop in the solution at high Peclet numbers (high velocity, low diffusivity, large finite elements). Several schemes were studied for the elimination of the oscillations and it was found that a streamline upwind procedure is quite effective in most cases.

FACTORS INFLUENCING THERMOMECHANICAL FAILURE OF FACE SEALS II

Interim Report #2
submitted to

Office of Naval Research
Contract No. N00014-81-K-0090
Period Covered: December 1, 1981 to November 30, 1982

by

Francis E. Kennedy, Jr.
Associate Professor of Engineering

and

John N. Grim and Roger P. Glovsky
Graduate Research Assistants

Thayer School of Engineering
Dartmouth College
Hanover, New Hampshire 03755

January 1983

Reproduction in whole or in part is permitted for
any purpose by the United States Government

FOREWORD

Work at the Thayer School of Engineering at Dartmouth College on this project has been supported by Office of Naval Research Contract No. N00014-81-K-0090. Mr. M.K. Ellingsworth of ONR is the contract monitor.

The authors gratefully acknowledge the cooperation of personnel from the David Taylor Naval Ship R&D Center, especially in the early stages of the project. In particular Mr. Sidney A. Karpe of DTNSRDC assisted in microscopic observations and contributed to many fruitful discussions about microscopic aspects of thermocracking.

Mr. Victor A. Surprenant of Dartmouth College assisted in metallography and in interpreting the microscopic observations.

Face seals for the experimental phase of the project were contributed by EG & G Sealol, Inc., H.F. Greiner Vice President and Chief Engineer.

The principal investigator (FEK) gratefully acknowledges the use of the computer facilities at the Laboratoire de Mécanique des Contacts, INSA, Lyon, France for a portion of the computational work on this project.

DTIC COPY INSPECTED 2

Accession For
NTIS GRA&I ☑
DTIC TAB ☐
Unannounced ☐
Justification
By
Distribution/
Availability Codes
Dist | Avail and/or Special
A

TABLE OF CONTENTS

Page

INTRODUCTION -- 1

SUMMARY OF PREVIOUS RESULTS ON CONTRACT N00014-81-K-0090 -------------- 3

EXPERIMENTAL STUDY OF CONTACT PATCHES IN FACE SEALS ------------------ 5

EXPERIMENTAL APPARATUS --- 6

TEST PROCEDURES AND MATERIALS ------------------------------------- 11

RESULTS AND DISCUSSION OF EXPERIMENTAL STUDY ------------------------ 15

    Rotating mating ring-dry - 15

    Rotating carbon primary ring-dry - - - - - - - - - - - - - - - - 24

    Rotating metallic ring with sealed fluid - - - - - - - - - - - - 24

CONCLUSIONS FROM EXPERIMENTAL STUDY --------------------------------- 26

ANALYTICAL STUDY OF TEMPERATURES NEAR CONTACT PATCHES ----------------- 27

FINITE ELEMENT THERMAL ANALYSIS PROGRAM (THERMAP) -------------------- 29

FACTORS INFLUENCING SURFACE TEMPERATURES IN FACE SEALS ---------------- 33

EFFECT OF MOVING SURFACE VELOCITY ON THERMAL ANALYSIS ----------------- 38

    Evidence of numerical instabilities at high velocity - - - - - - - 38

    Techniques for handling convective-diffusion equations - - - - - - 43

    Application of upwinding techniques to THERMAP - - - - - - - - - - 47

CONCLUSIONS FROM ANALYTICAL STUDY ----------------------------------- 53

REFERENCES -- 54

APPENDIX A THEORETICAL DEVELOPMENT OF EQUATIONS ---------------------- 56

APPENDIX B THERMAP FLOWCHART -- 62

APPENDIX C USER INSTRUCTIONS FOR THERMAP ---------------------------- 63

APPENDIX D LIST OF PUBLICATIONS AND PRESENTATIONS RESULTING FROM THIS SEARCH ---------- 66

APPENDIX E DISTRIBUTION LIST -- 67-72

LIST OF FIGURES

Figure | Page

1. Schematic diagram of contact probe (above) Idealized output signal (below). 7

2. Photograph of stationary carbon primary seal ring containing contact probe, in its holder. Electrical contact brush, which slides against mating ring, is also included. 10

3. Schematic diagram of entire test system. 12

4. Comparison between contact probe output (Fig. 4a) and appearance of mating ring surface (Fig. 4b). Test A, 440C stainless steel mating ring, 188.5 rad/sec, dry. 16

5. Comparison between contact probe output (Fig. 5a) and appearance of mating ring surface (Fig. 5b). Test B, 440C stainless steel mating ring, 188.5 rad/sec, dry. 16

6. Comparison between contact probe output (above) and thermocouple output (below). Test E, 440C stainless steel mating ring, 125.7 rad/sec, dry. 18

7. Sequence of output traces from contact probe, showing growth of contact patches to steady state size. 21

8. Contact probe output (steady state). Beryllium copper mating ring, 188.5 rad/sec, Test H. 22

9. Contact probe output (steady state). 52100 bearing steel mating ring, 188.5 rad/sec, Test O. 22

10. Sketch of primary seal ring, showing section studied in thermal and stress analyses. 30

11. Finite element mesh for mechanical face seal. 31

12. Isotherms in mating and primary seal rings for case of Figure 11. 34

13. Study of velocity effect in frictionally heat generating contact problem. 40

14. Finite element test models for study of velocity effect. 45

LIST OF TABLES

Table No.		Page
1.	Properties of mating ring materials used in this study.	13
2.	Characteristics of steady-state contact patches for various mating ring materials.	20
3.	Parametric study for mechanical face seal analysis.	37
4.	Results of thermal analyses of moving slab subject to distributed heat source.	44
5.	Results of one dimensional thermal analysis with moving heat source.	48
6.	Moving slab with distributed heat source - results of analysis with upwinding.	49

INTRODUCTION AND BACKGROUND

Introduction

Mechanical face seals are designed to prevent fluid leakage around rotating shafts at points where the shaft passes through a stationary housing or pressure vessel. They have proven to be the most effective type of seal for severe applications involving high fluid pressures, high shaft speeds, or a combination of these conditions. Unfortunately, as the severity of the application increases, the frequency of seal failure, as indicated by excessive leakage and/or excessive seal friction, also increases. Such failures should be avoided, if possible, especially in marine applications where the seal prevents intrusion of sea water along a rotating propeller shaft.

Several of the most common modes of face seal failure are caused by a combination of high temperature and high stress in the seal components. These thermomechanical failure modes, which include thermocracking, or heat checking, and warping of the mating ring, are often responsible for excessive seal leakage, excessive wear of the primary ring, and, occasionally, fracture of the mating ring. Attempts to eliminate thermocracking and related thermomechanical problems in face seals have not been completely successful, primarily because our understanding of these mechanisms is very limited. The goal of this research has been to gain a better understanding of factors affecting thermocracking and other related failure mechanisms in mechanical face seals.

It has been known for a number of years that thermocracking in face seals is caused by thermal stress resulting from frictional heating. Several studies of the problem [1,2] resulted in the proposal of material parameters by which a material's resistance to thermocracking can be predicted. Those studies did not really establish a mechanism for thermocracking, however, and they assumed that temperature and stress distributions on the sliding interface are both uniform - an assumption which has since proven to be false.

In order to achieve good performance from a mechanical face seal, the sealing surfaces of both primary seal ring and mating ring are lapped to a high degree of flatness during production. Despite this, a very slight amount of initial waviness remains and this waviness has been observed to grow during seal operation [3]. One consequence of this waviness is that frictional surface tractions are not uniformly distributed over the sealing interface and this results in circumferential variations in frictional heating of the seal rings. It was shown by Burton and his co-workers [4] that under certain conditions this nonuniform heating may lead to even more concentration of friction and frictional heating, and to the formation of hot, highly stressed contact patches, or thermal asperities. Later analytical work determined the influence of operating variables, such as velocity, and of material parameters, such as thermal conductivity, modulus of elasticity, coefficient of thermal expansion, wear resistance and friction coefficient, on this unstable process of transition from nominally flat to highly deformed surfaces [5-7].

These analytical studies showed conclusively that this unstable condition, called thermoelastic instability, could occur in face seals. It was hypothesized that the stresses and temperatures near the resulting thermal asperities could be responsible for thermocracking and other modes of seal failure. There was some evidence, based on observation of disassembled face seals after failure, that this was in fact what had occurred [8]. The hypothesis was not proven conclusively because several things were missing: first, experimental evidence that small, hot contact patches resulting from thermoelastic instability actually occur in operating face seals and, if so, information about factors influencing the size, location, and number of these patches and contact conditions within them; and second, a study showing how conditions near the contact patches can lead to the onset of thermocracking. This research project has been attempting, with some success, to provide this information and to establish a firm basis for recommendations for the design of face seals which would not be subject to a high incidence of thermomechanical failure.

SUMMARY OF PREVIOUS RESULTS ON CONTRACT N00014-81-K-0090

Since December 1, 1980, work has been in progress at Thayer School of Engineering on ONR Contract N00014-81-K-0090. During the first year, the research was directed at learning the root causes of thermocracking, whether these causes are related to non-uniformity of contact at the seal interface, and what material parameters have the most influence on thermocracking mechanisms. The research included both analytical and experimental activities aimed at accomplishing these goals. Most of the results achieved during the first year of the research program have been published elsewhere [9,10]. Those results will be summarized here.

The first phase of the work, accomplished with the aid of personnel at the David Taylor Naval Ship R&D Center in Annapolis, involved the examination of marine seal components which have exhibited thermocracking. Macroscopic and microscopic examination of the metallic seal rings showed that most thermocracks are radial in nature and initiate at carbide particles on the seal surface of the cast cobalt-based alloy rings [9]. The cracks, which are distributed relatively uniformly in the circumferential direction on the seal face, appear to initiate and propagate in a brittle manner in a tensile mode (Mode I). There was evidence on the seal surfaces that localized contact conditions had occurred in thermocracked regions, with both deformation and temperature in the contact region being rather severe.

The next phase of this research was an analytical study which aimed to determine how localized contact patches at the seal interface could lead to the onset of thermocracking. The finite element method was chosen and a finite element thermal analysis program was developed for use in calculating surface temperature distributions in sliding seals [11]. This program, THERMAP, was used along with a finite element stress analysis program, FEATS, to determine temperature and thermal stress distributions near contact patches on the seal ring surface [9,10]. It was found that very high temperatures occur at the contact patches owing to frictional heating. The regions affected by these high temperatures are quite small, but thermal stresses in those regions are large. The stresses are compressive, however, so cannot directly cause thermocracks of the type observed in our studies. It was concluded that these large compressive thermal stresses cause substantial plastic deformation near contact patches. Upon movement of the contact patch, residual tensile stress would result which could easily cause cracks like those observed, especially if the seal face material is brittle or contains a brittle phase [9].

The analytical study resulted in a proposed thermocrack mechanism which could account for all observed characteristics of thermocracks. The analysis relied, however, on a crucial assumption - that the formation of localized contact patches, or thermoelastic instabilities, precedes thermocracking. Although such small, highly loaded, contact patches had been observed in various laboratory configurations by other researchers, there had been no direct observation of thermoelastic instabilities in face seals. The only evidence had been ex-post-facto, as in the early phase of this work.

EXPERIMENTAL STUDY OF CONTACT PATCHES IN FACE SEALS

Although the hot spots resulting from thermoelastic instability have been studied analytically by a number of researchers [6], there has been little direct evidence of their existence in seals. The most dramatic experimental verification of thermoelastic instabilities, by Dow and Stockwell [12], was for a case of a thin blade loaded against the outside of a rotating drum. The blade was oriented parallel to the axis of the drum so the drum surface was moving perpendicular to the blade. The results of that study are not directly applicable to face seals because the kinematics are different from those in a face seal. Banerjee and Burton [12] conducted tests on a ring on disk configuration kinematically similar to a face seal, and observed the formation of thermoelastic instabilities. The materials used in their tests, aluminum ring on glass disk, are different from those used in face seals, however, so again the direct applicability of their results to face seals is open to question. Netzel [8] has reported evidence of hot spot formation due to thermoelastic instability in a variety of face seals. His observations were made on seals which had been disassembled after suffering from excessive wear, unacceptable leakage, and/or high frictional power loss. The observations provided much evidence that instabilities had occurred during operation of the seals and that the resulting hot spots had contributed to the seal failure. They did not provide, however, the final proof of the presence of thermoelastic instabilities in operating face seals - observation of the hot spots while they were occurring.

The purpose of this phase of the study was the development of an experimental technique to observe the hot contact spots resulting from thermoelastic instability during operation of actual mechanical face seals. The technique could then be used to determine the size of the spots, the motion of the spots relative to each of the two contacting seal faces, and the influence of various operating and material parameters on hot spot characteristics. It was also desired to devise and implement a means for measuring temperature of the contacting surfaces within the hot spots.

EXPERIMENTAL APPARATUS

A monitor was desired which could determine the number, size, location, and relative motion of patches of contact on the interface of an actual face seal during operation. It was also desired that the monitor be easy to use and not modify the operating characteristics of the face seal. Temperature measurement within the contact patch was also desired.

Although a variety of contact probes are available, none were deemed suitable for this application and it was instead decided to design and construct one. Recall that the major characteristic of thermoelastic instabilities is nonuniform contact. It follows that the areas of contact and non-contact, if suitably different, would act like the opening and closing of an electrical switch if current were selectively passed through a narrow interfacial region between primary and mating seal rings, provided that one of the rings is conductive. Implementation of this idea is described schematically in Figure 1. A fine wire is implanted in, but insulated from, the stationary seal ring (carbon in this case). The probe is then levelled flush with this seal surface through polishing techniques. A graphite electrical brush is placed against the outer diameter of the rotating mating ring to inject current into the system. Current flows from the brush through the ring to the probe wire only when there is direct contact at the probe location. If small thermal asperities, resulting from thermoelastic instability, are present on the mating ring surface, current will flow through the system only when the asperities are in contact with the probe wire. An intermittent output (current flow) will thus be produced (Figure 1). If the contact patches are stationary with respect to the moving seal ring, the output will be periodic in nature, repeating once each revolution.

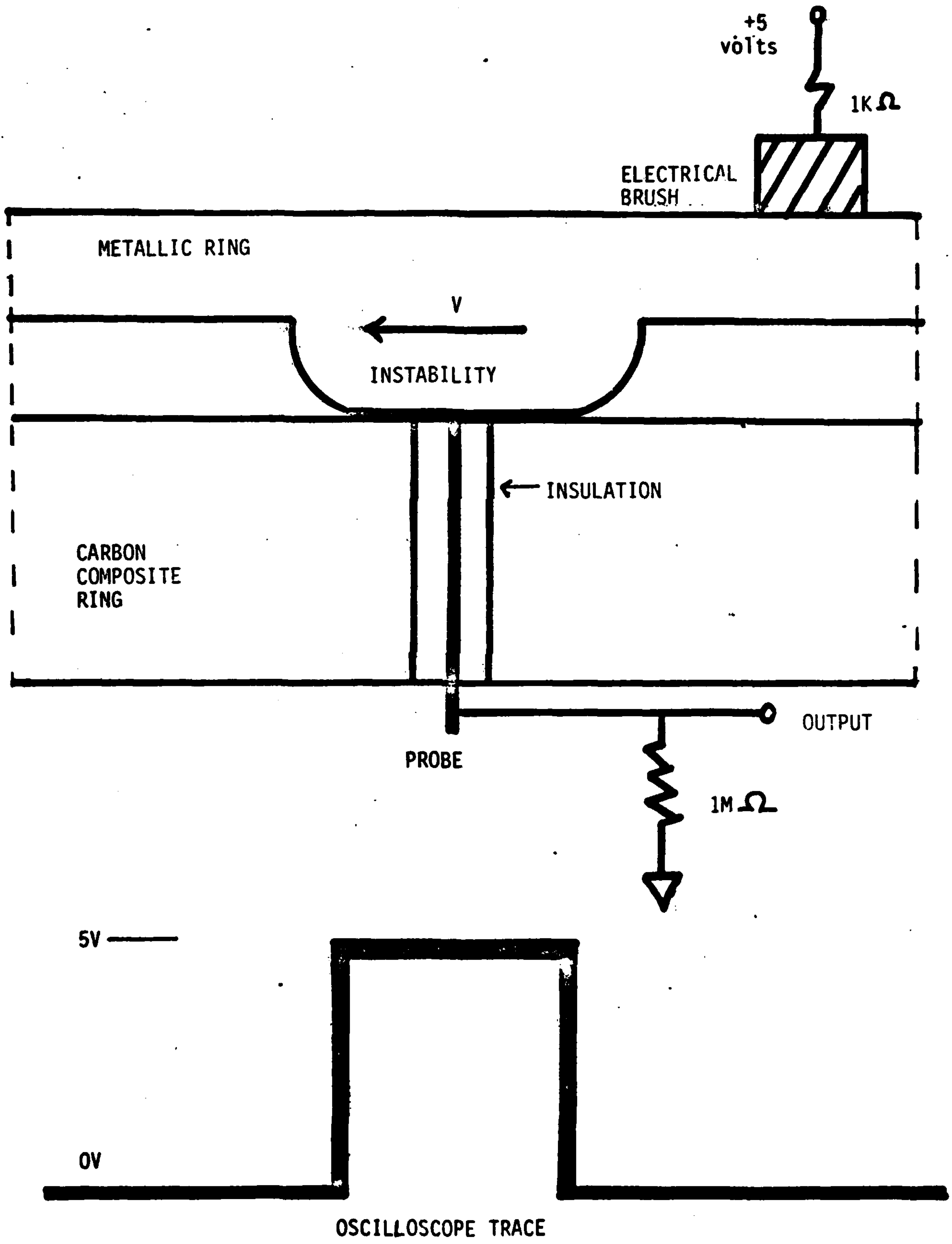
+5 volts
1KΩ
ELECTRICAL BRUSH
METALLIC RING
V
INSTABILITY
INSULATION
CARBON COMPOSITE RING
OUTPUT
PROBE
1MΩ
5V
0V
OSCILLOSCOPE TRACE

Figure 1 Schematic diagram of contact probe (above). Idealized output signal (below).

The seals used in this test program were commercially-available mechanical face seals designed for turbine engine applications. The seal has a carbon graphite primary ring and a mating ring made of 440C stainless steel. The sealing surface has a diameter of approximately 5 cm. and a width of about 2.5 mm. To implant the contact probe, a .22 mm hole was drilled through the carbon ring and a .178 mm diameter constantan wire, surrounded by a thin coating of epoxy insulation, was embedded in the hole with epoxy. The sealing surface of the ring was ground, lapped and polished to a surface finish of less than .3μm to insure that the end of the wire was flush with the surface and that the surface was at least as flat as a new commercial seal face.

It should be noted that although the above description was for insertion of the contact probe in the carbon ring to monitor contact between it and contact patches on the moving metallic mating ring, a similar procedure can be, and indeed was, followed in which the rings were switched. That is, a contact probe was embedded in the stationary metallic ring to monitor contact patches on the moving carbon ring. In this way a complete mapping of contact patch sizes and their relative motion relative to each of the seal rings could be obtained. This was possible in this case owing to the good electrical conductivity of both ring materials.

An electrical brush was designed to supply the rotating seal ring with a 1 milliamp current at 5 volts. The graphite brush and its support rod were spring loaded to provide a constant contact force between the brush and the outer diameter of the rotating seal ring. Both seal rings were supported in specially designed holders, each of which could accommodate either carbon or metallic ring. Each holder contained a plexiglass insulating disk to prevent current leakage from metallic components of the holders to ground. The lower holder also contains a means for introduction of pressurized fluid to the interior of the seal. Figure 2 shows a carbon primary seal ring, with contact probe, in position in the lower holder.

The upper holder, containing the rotating seal ring, was attached to the spindle of a drill press. The drill press allowed variation of the rotational speed of the moving ring in 8 speeds ranging from 15.7 $^{rad}/sec$ to 188.5 $^{rad}/sec$, (surface velocity of moving ring ranged from .393 $^{m}/sec$ to 4.71 $^{m}/sec$). The drill press also allowed control of the contact pressure at the seal interface by means of axial force application. Although the spindle speed remained approximately constant during a test, a small variation in speed would produce a drift in the output signal which could cause errors in the determination of contact patch location. To overcome this, a simple tachometer was attached to the spindle to trigger the oscilloscope trace. The tachometer consisted of a notched circular plate attached to the spindle shaft and rotating between a stationary LED light source and a light receptor. Once each revolution the rotating notch allows the passage of photons to the receptor and this generates a pulse to trigger the oscilloscope. Since the trigger always occurs at the same position on the ring circumference, the output signal remains stationary with respect to the rotating seal ring. Any movement of the output pulses therefore represents a movement of the contact patches with respect to the moving ring and that movement can be continuously monitored.

The problem of measuring the seal surface temperature within the contact patches was solved by using a dynamic thermocouple. A thermocouple is formed by the junction of two dissimilar metals, with the voltage difference between the metals being linearly related to the temperature difference between the hot junction and the other, cold, junction of the thermocouple circuit. In a dynamic thermocouple one of the two metals at the hot junction is moving relative to the other. In this case the constantan probe wire served as one side

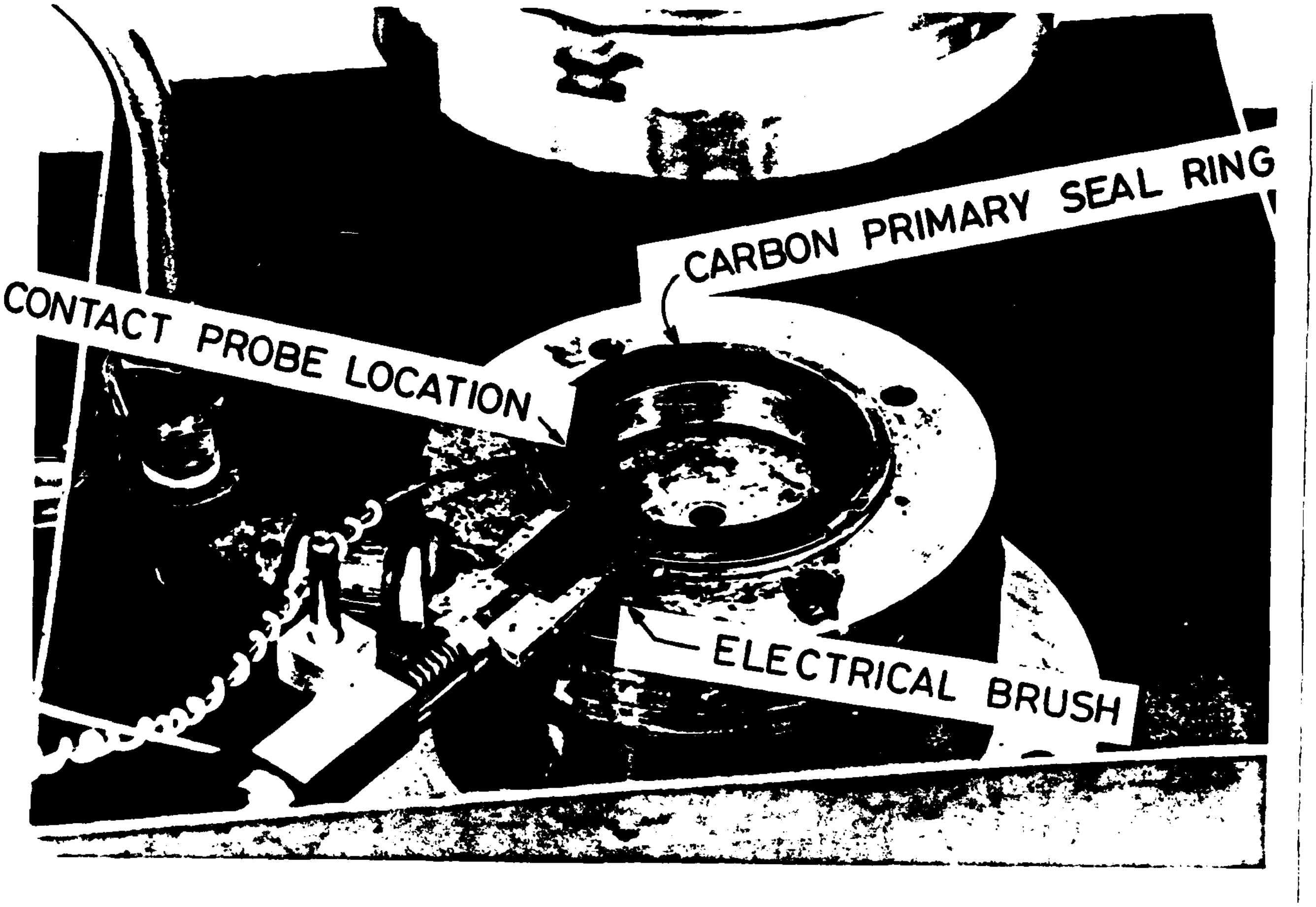
CARBON PRIMARY SEAL RING
CONTACT PROBE LOCATION
ELECTRICAL BRUSH

Figure 2 Photograph of stationary carbon primary seal ring, containing contact probe, in its holder. Electrical contact brush, which slides against mating ring, is also included.

of the thermocouple circuit while the metallic mating ring, provided it was an iron-or-copper-based material, could serve as the other. With the voltage source through the graphite brush turned off, contact between a thermal asperity on the moving metallic ring and the probe wire constitutes a thermocouple junction and the small resulting voltage between mating ring and constantan wire is proportional to the junction temperature. The junction voltage was measured using a potentiometer-amplifier circuit. Shielding of all wires was used to limit signal noise, but the thermocouple output signal, being of low input voltage, was still of lower quality than that from the contact probe. The thermocouple was calibrated by monitoring its static response to several known temperatures (0° and 100°C).

A test chamber was built around the lower seal holder to collect leakage of the sealed fluid. At the base of the chamber was a ball and seat which maintained alignment between primary and mating rings. The entire lower part of the assembly - stationary seal ring and holder, test chamber, and ball and seat system - rests upon a thrust bearing to allow free rotational motion. The rotation is impeded by two strain-gaged cantilever arms fixed to the drill press platform. The output from the strain gages was calibrated to enable determination of frictional torque. The normal force applied to the seal faces was applied by hanging known weights from a pulley attached to the drill spindle lowering mechanism. From this known normal force and the measured frictional torque, a friction coefficient could be determined.

A schematic diagram of the entire test apparatus is shown in Figure 3. More details of the test system can be found in Reference 14.

TEST PROCEDURES AND MATERIALS

Three different types of tests were run in this program:

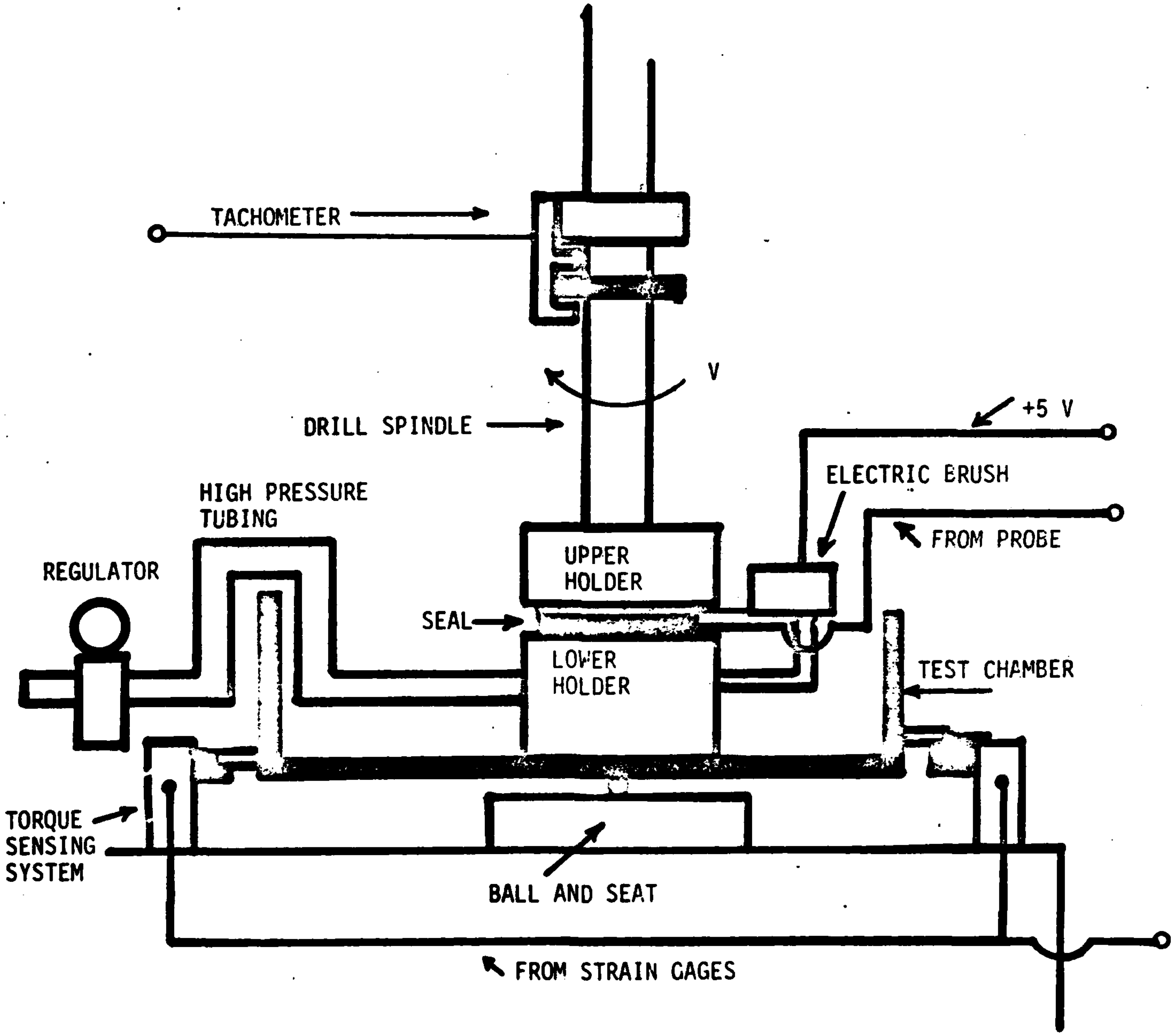
TACHOMETER
V
DRILL SPINDLE
+5 V
ELECTRIC BRUSH
HIGH PRESSURE TUBING
FROM PROBE
REGULATOR
UPPER HOLDER
SEAL
LOWER HOLDER
TEST CHAMBER
TORQUE SENSING SYSTEM
BALL AND SEAT
FROM STRAIN GAGES

Figure 3 Schematic diagram of test apparatus

TABLE 1

Properties of Mating Ring Materials Used in this Study

Material	Rockwell Hardness	Modulus of Elasticity (GPa)	Thermal Conductivity (W/M·K)	Coefficient of Thermal Expansion (10-6/°C)
440C Stainless Steel	R_C 58	200	24.2	100.8
Beryllium Copper	R_C 38	131	100.5	167.4
52100 Bearing Steel	R_C 62	207	38.1	126.2

(1) Rotation of three different metallic mating rings against a stationary carbon primary ring at three different test speeds in air under dry, unpressurized conditions.

(2) Rotation of the carbon ring against a stationary mating ring under dry, unpressurized conditions.

(3) Rotation of a metallic ring against the stationary carbon ring with pressurized water as a sealed fluid.

The first series of tests used mating rings made from 440C stainless steel (the production material), hardened beryllium copper, and 52100 bearing steel. The properties of these materials are given in Table 1. Each of the rings was rotated at three different speeds: 62.8 ^{rad}/sec, 125.7 ^{rad}/sec, and 188.5 ^{rad}/sec.

To answer the question of the ring surface upon which the thermal asperities resided, the carbon ring was also rotated. These tests were done with a stationary metallic ring (440C stainless steel) and with the carbon ring rotating at four different speeds, the three listed above plus 31.4 ^{rad}/sec. In this case the contact probe was embedded in the stainless steel ring, but insulated from it.

The only tests with pressurized water were run with a rotating mating ring made from 440C stainless steel and a stationary carbon ring. The rotational speed was 125.7 ^{rad}/sec. Conventional tap water at a pressure of .35 MPa was introduced at the interior of the face seal after the seal rings were in contact but before rotation began.

The test procedure was as follows. Prior to a test both mating and primary seal ring were lapped, polished to a surface roughness of .25μm or better, and cleaned with acetone. Proper functioning of the contact probe was insured by microscopic examination and an electrical check, and the temperature circuitry was checked for electrical bias. Torque measuring circuitry was also checked.

The drill spindle was lowered and the desired normal force (65N in most cases) was applied. The drill press was turned on, with the rotational speed having previously been set to the desired value. With the tachometer/trigger system on, monitoring of the contact probe output on the oscilloscope began. At desired time intervals, photographs of the output trace were taken and the then current source was turned off so that the thermocouple output could be monitored. Photographs of that output signal were also taken. The tests continued until either the signals remained unchanged for at least 15 minutes or until the contact probe stopped functioning (see below). Most tests lasted at least 30 minutes.

RESULTS AND DISCUSSION OF EXPERIMENTAL STUDY

Rotating mating ring - dry. The first tests, with a stainless steel mating ring rotating at 188.5 $^{rad}/sec$, were aimed at proving the viability of the contact probe, which was located in the stationary carbon ring. As noted earlier, the mating ring had been lapped and polished prior to testing. Despite this, the contact probe displayed evidence of distinct contact patches immediately upon operation (with no sealed fluid). In the first test there was immediate indication of two distinct contact spots, one well-defined and the other, about 120° around the circumference, smaller in size. Soon thereafter, a third spot, about 120° from each of the first two, became visible. These three spots grew slightly in size until they reached, after about 15 minutes of testing, the size indicated in Figure 4(a). The figure shows that the output from the contact probe is approximately a squarewave form with three peaks, 100-120° apart, which repeat with each revolution of the mating ring. This indicates that three patches of contact are present on, and rotating with, the mating ring surface.

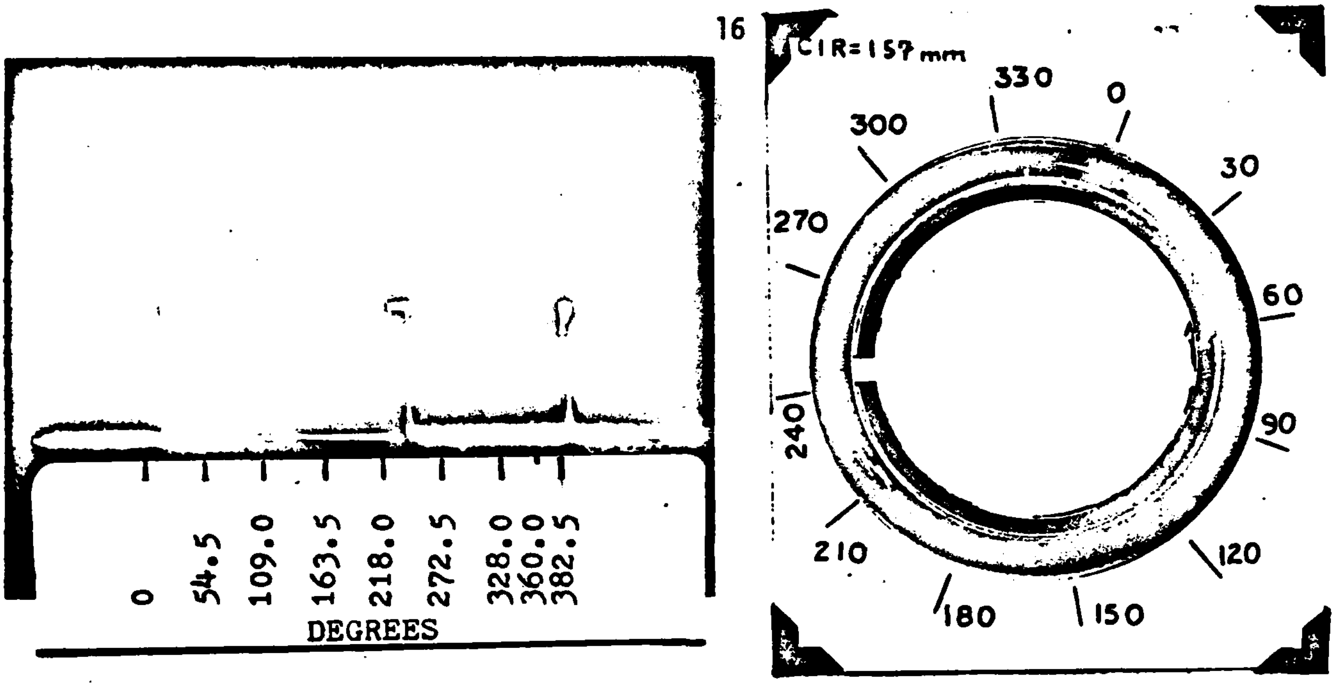

Figure 4a

Figure 4b

Comparison between contact probe output (4a, left) and appearance of mating ring surface (4b, right).
440C Stainless steel mating ring, 188.5 rad/sec, dry.

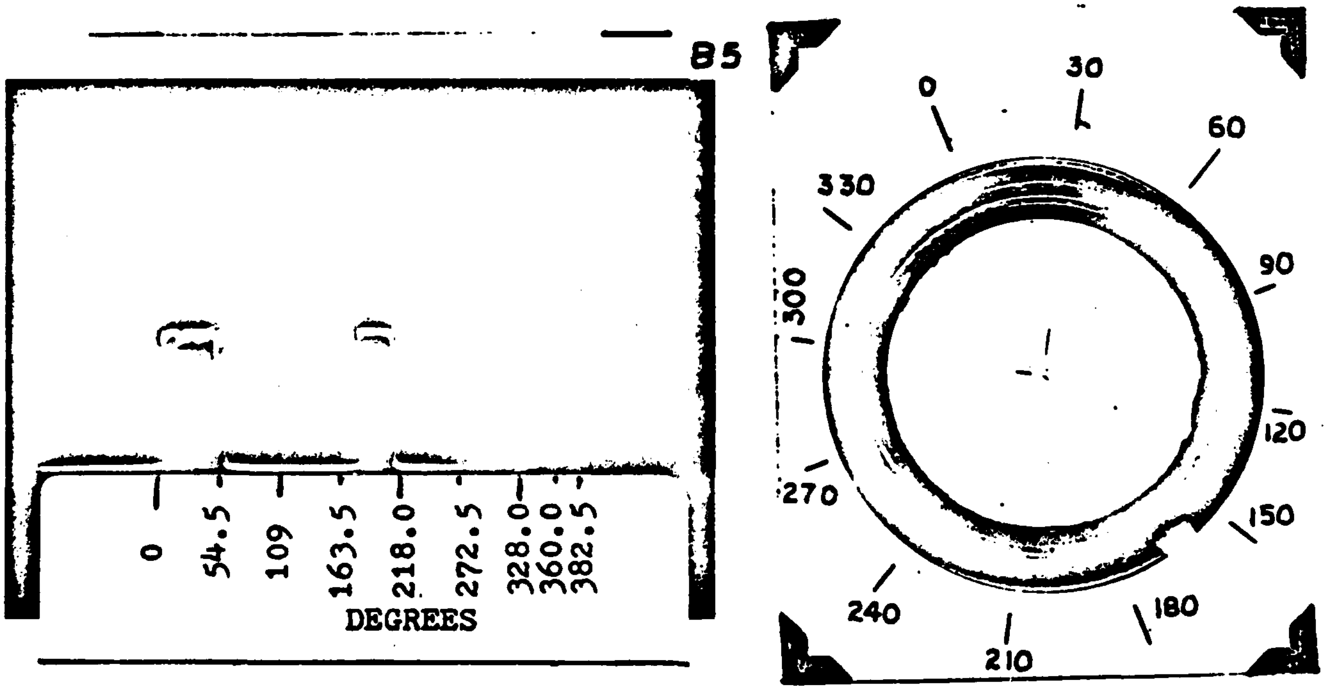

Figure 5a

Figure 5b

Comparison between contact probe output (Fig. 5a, left) and mating ring surface appearance (Fig. 5b, right).
440C Stainless steel mating ring, 188.5 rad/sec, dry.

The test was stopped, and the seal disassembled, just after the photo of Figure 4(a) was taken. Observation of the mating ring surface showed that there were three distinct wear patches on the surface (see Figure 4(b)). Note the very close correlation between the size and distribution indicated by the contact probe and that visible on the ring surface.

A second test, under the same conditions, but with freshly polished seal surfaces, yielded the results shown in Figure 5. Again there were two small spots apparent immediately after rotation began, but this time they were 180° apart and those two spots grew to the steady state size shown in Figure 5(a). The mating ring surface, upon disassembly of the seal soon after Figure 5(a) was taken, showed evidence of contact in patches of about the same size and in the same location as those indicated by the contact probe. This test, and that shown in Figure 4, show conclusively that contact conditions in a face seal, as determined either by the contact probe or by seal disassembly and observation, are not uniform, but that the number of patches of actual contact cannot be uniquely predetermined.

Although the temperature probe (dynamic thermocouple) was not in operation in the tests described above, it was used successfully in numerous other tests. Results of one such test are shown in Figure 6. It can be seen that the regions of temperature indication coincide with the contact patch locations (no thermocouple junction is formed where contact does not exist), and that the temperature generally reaches a maximum near the trailing edge of the contact patch. This is in agreement with theoretical predictions of surface temperature in fast moving contacts in seals [9].

An extended series of tests was run with three different mating ring materials, and at three different mating ring speeds. In all tests, no matter what the mating ring material or the sliding speed, the contact probe showed

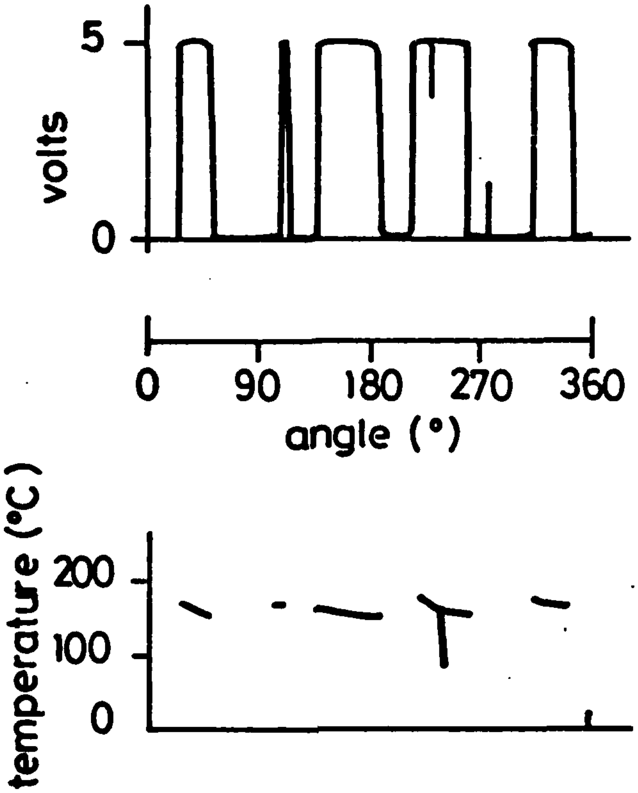

Figure 6 Comparison between contact probe output (above), and thermocouple output (below). Test E, 440C stainless steel mating ring, 125.7 rad/sec, dry.

evidence of small, distinct contact spots being present as soon as seal operation began. This occurred in spite of all our efforts to lap and polish the seals before operation and it is probably due to a very slight initial waviness of the seal faces. Very soon after the test began, however, the spot size began to grow, both by expansion of the patches and by formation and joining together of new contact spots. A steady state patch size, or at least one in which no significant growth occurred during a 15 minute period, was reached within 30-60 minutes for all seals. In each case these steady state patches appeared to be rotating with the mating ring, showing no motion with respect to that ring. The growth of asperities from their initial size (within 1 minute) to their steady state size (after about 30 minutes) is depicted in Figure 7.

A summary of the characteristics of the steady state contact patches for each of the test cases is given in Table 2, with typical results for each of the seal materials being given in Figures 7(b), 8, and 9. A study of the results shows that although there is no unique set of patch characteristics associated with any set of test parameters, there are some significant trends. For a given seal velocity, the 52100 bearing steel ring tends to have the smallest patch lengths, the highest patch temperatures and generally the most patches of contact, while the beryllium copper ring tends to have the largest and coolest patches. Complete contact over the entire circumference (157 mm) was obtained in a test at 125.7 $^{rad}/sec$ with the beryllium copper ring, but only at the lower speed (62.8 $^{rad}/sec$) with the 440C stainless steel ring, and never with the ring made from 52100 bearing steel. In general, higher patch temperatures accompany higher velocities and/or smaller spot sizes. The friction coefficient was found to be approximately the same for all materials and velocities in this series of tests, ranging from .10 to .12. The total heat generation rate is, therefore, approximately proportional to velocity. The measured patch

TABLE 2

Characteristics of Steady-State Contact Patches for Various Mating Ring Materials

(Rotating Mating Ring - No Sealed Fluid)

Test	Mating Ring Material	Rotational Speed (rad/sec)	Number of Contact Patches	Patch Lengths (mm)	Patch Temperature (average) (°C)
A	Stainless Steel	188.5	3	3.3, 4.8, 3.3*	—
B	"	"	2	23.8, 13.8	—
C	"	"	1**	7.6**	205
D	"	"	3	24.8, 19.0, 26.2	190,190,190
E	"	125.7	5	10.4, 3.8,25.1,18.8,13.5	170,170,160,150,170
F	"	"	3	15.1,10.1,32.0	190,190,185
G	"	62.8	1	157	155
H	Beryllium Copper	188.5	1	133	140
I	"	"	2	21.4,52.4	—
J	"	"	3**	9.5,11.0,13.3	—
K	"	125.7	2	87.9,47.1	110,120
L	"	"	1	157	130
M	"	"	2**	53.4,34.6**	90,95
N	"	62.8	3	51.8,7.0,59.7	90,85,85
O	52100 steel	188.5	4	11.9,19.0,18.1,19.0	215,195,150,175
P	"	"	2	33.3,23.8	—, 215
Q	"	"	4	8.1,3.3,7.1,7.6	—
R	"	125.7	1**	6.3**	215
S	"	"	3	23.6,18.8,18.8	—
T	"	62.8	2	9.5, —**	195, —

*This test was foreshortened, patch lengths had not increased to steady-state values.

**There was evidence that other patches were present, but their characteristics could not be measured.

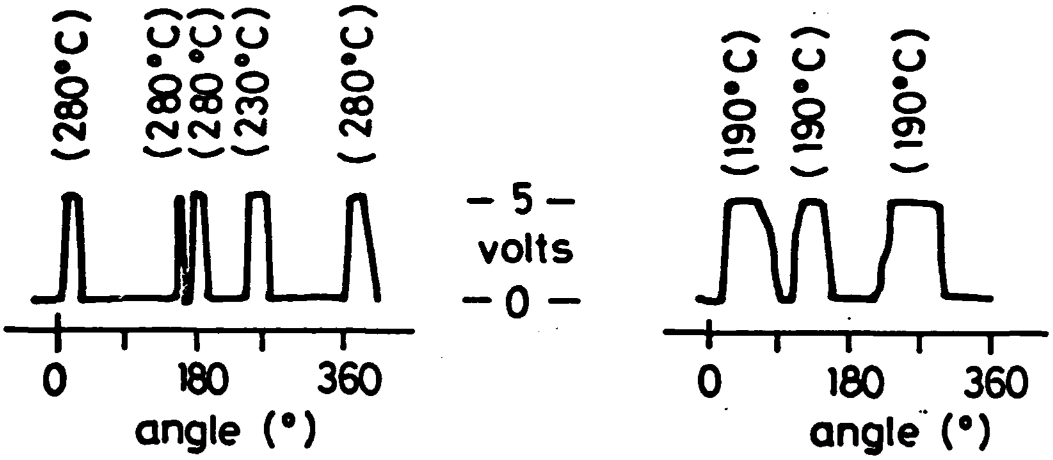

Figure 7 Sequence of output traces from contact probe, showing growth of contact patches to steady state size. Surface temperatures, shown above contact probe output, decrease as patch sizes increase.
Stainless steel mating ring, 188.5 rad/sec.

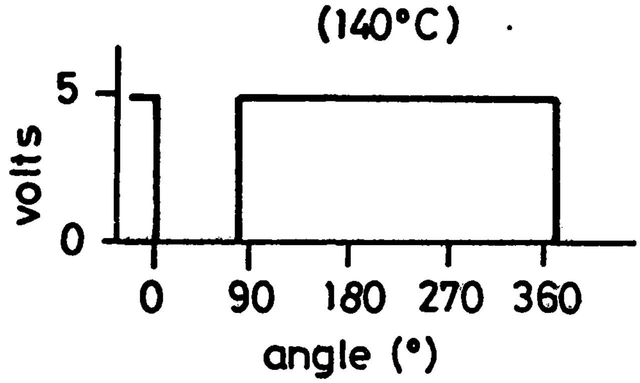

Figure 8 Contact probe output (steady state) Beryllium copper mating ring, 188.5 rad/sec, test H.

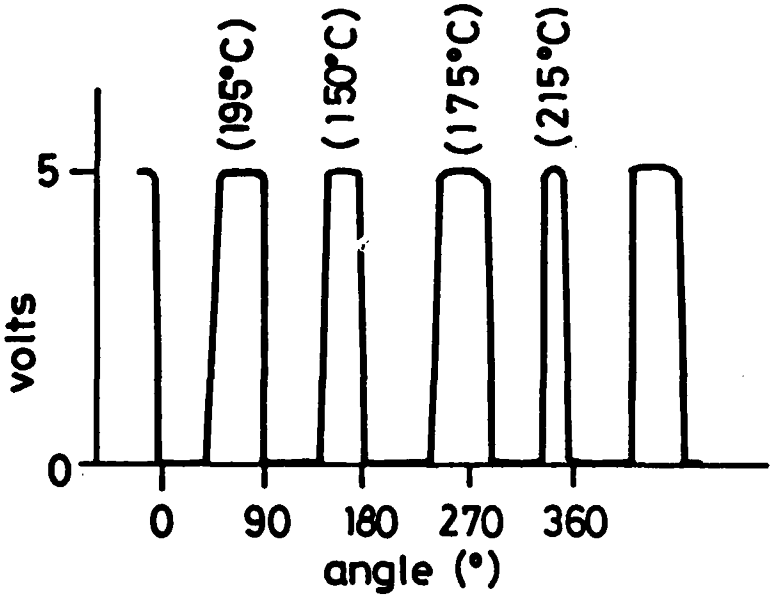

Figure 9 Contact probe output (steady state) 52100 bearing steel mating ring, 188.5 rad/sec, test O.

temperatures are not directly porportional to the velocity though, because at a given total heat generation rate temperature is increased by a decrease in spot size or by a decrease in velocity [9].

In general, it can be stated that the long-term presence of thermal asperities (or thermoelastic instabilities) is suppressed more by beryllium copper than by stainless steel and least with 52100 alloy steel. The major influences promoting the growth of thermal asperities are heat conduction and wear. In Table 1 it can be seen that beryllium copper is the most conductive and softest of the three materials. The higher conductivity of beryllium copper aids in the dissipation of frictional heat, leading to lower hot spot temperatures than with the other materials. This in turn leads to less thermal dilatation and less driving force for thermal asperity formation. The lower hardness of beryllium copper leads to lower wear resistance and, therefore, easier removal of thermal asperities once they have formed. 52100 bearing steel, the most wear resistant of the three materials, tends to have thermal asperities which are resistant to growth by wear. That material also has the highest product of modulus of elasticity and thermal expansion coefficient, a factor which determines the stress and deformation response of a material to a temperature rise.

Burton [6] has stated that patch length is proportional to thermal conductivity and inversely proportional to sliding velocity, friction coefficient, and the product of modulus of elasticity and thermal expansion coefficient, and that patch length is decreased by increased wear resistance. Although the parametric influences in our tests are similar to those predicted by Burton, attempts to use his equation [6], which did not include a wear coefficient term, to predict our measured contact lengths proved fruitless. The sizes of thermal asperities predicted by the Burton equation were much smaller than those measured experimentally. In addition, that equation predicted that 52100 bearing steel has a larger patch size at a given velocity than 440C stainless steel, in direct opposition to our experimental observations. Perhaps these inaccuracies could be remedied by the inclusion of a determinable wear resistance term in Burton's equation.

Rotating carbon primary ring - dry. No motion of the contact patches relative to the metallic mating ring was noted in the first test series, in which the mating ring was rotating. In this set of tests a contact probe was placed in the stationary mating ring and the carbon primary ring was rotated. The aim was to see if, under those different kinematic conditions, there was any motion of the contact patches relative to the metallic mating ring. The results were negative. Either an indication of contact was observed at the contact probe, in which case it remained in contact throughout the 30 minute test, or no contact was observed at the probe location throughout the test. Similar results were found at all velocities, which ranged from 31.4 to 188.5 $^{rad}/sec$. Upon disassembly of the seal after the tests, however, there were worn areas on the mating ring surfaces, similar to those shown in Figures 4(b) and 5(b), in many cases. Thus, there was evidence that thermal asperities had been present on the mating ring surface, sometimes at the probe location and sometimes elsewhere, but the bumps did not seem to be moving on the mating ring.

The fact that these tests produced no good evidence that thermal asperities were present on, and rotating with, the carbon ring surface, is probably due to the relatively low wear resistance of the carbon material. Any such thermal bumps which may have formed on that surface were probably worn away nearly immediately.

Rotating metallic ring with sealed liquid. Most face seals are used to seal a liquid, not dry air as in the earlier tests, so the evidence of contact patch formation presented earlier does not necessarily apply to those liquid lubricated seals. For that reason a series of tests was run using the same test apparatus but with pressurized water being present, as a sealed fluid, at the inside diameter of the seal. A contact probe was implanted in a stationary carbon primary ring, while a 440C stainless steel mating ring was rotated. The seal faces were prepared, and the tests run, in the same manner as in the dry tests.

Results of these liquid lubricated tests were much less satisfactory than those of the dry tests. During seal operations, water was present as a very thin lubricating film between the seal faces. This water, which was slightly ionized and thereby conductive, enabled current to flow between the contact probe and the mating ring even when no contact occurred at the probe location. This current leakage produced a continuous output signal of nearly 5 volts, and this just about obliterated output signals from the contact probe. There was, however, some evidence that signals from contact patches were superimposed on the leakage signal. The signals suggest that the fluid film is continually being broken by small patches of solid-to-solid contact. The contact patches appeared to be transitory in nature, however, in contrast to the long lasting, stable patches which were observed in dry contact. It is possible that the liquid film aids in the cooling of the hot contact patches, leading to a relatively short-lived existence of the patches.

Work is now in progress to overcome the current leakage problems encountered with liquid lubricated seals and to expand these preliminary results. It should be mentioned that somewhat similar, but unrelated, current leakage problems occurred in several dry tests, forcing the early curtailment of the test. In those cases the leakage was caused by wear debris from the carbon seal ring which formed a bridge from the constantan probe wire across the surrounding insulation to the carbon seal ring in which the wire was embedded. In those few cases the problem was remedied by a repolishing of the seal surfaces.

CONCLUSIONS FROM EXPERIMENTAL STUDY

1. A contact probe/thermocouple apparatus has been built which enables the monitoring of contact conditions on the sealing surfaces of mechanical face seals during seal operation. The probe system was applied successfully to measure the size, distribution, and surface temperature of patches of solid-to-solid contact on the seal faces.
2. Contact patches resulting from thermoelastic instabilities have been observed to exist on the surface of operating mechanical face seals under both dry and liquid lubricated conditions. At least in dry operation, the patches tend to remain stationary with respect to the metallic mating ring of the seal, whether that ring be stationary or rotating.
3. Contact patches observed on beryllium copper mating rings tend to be larger, fewer in number, and at a lower temperature than those found with mating rings made from 440C stainless steel or 52100 bearing steel. The 52100 rings had the smallest and hottest contact patches at all seal velocities.
4. Based on the results of these tests it appears that the mating ring materials most conducive to the formation of small, hot, long lasting contact patches (or thermoelastic instabilities) are those with low thermal conductivity, high wear resistance, and high modulus of elasticity and coefficient of thermal expansion. A combination of heat conduction and wear can lead to the enlargement of the contact patches, resulting in more uniform contact and lower contact temperatures. A decrease in velocity also results in more uniform contact, larger contact patches, and lower contact temperatures.

ANALYTICAL STUDY OF TEMPERATURES NEAR CONTACT PATCHES

The goal of this analytical study was the determination of temperature distributions in mechanical face seals. It was earlier [9,10] shown that these temperatures cause thermal stresses which are the probable cause of thermocracking of the seal faces. It was desired to determine the influence of various operating and material parameters on seal temperatures. To accomplish these goals, a thermal analysis of the contacting rings was carried out using finite element methods.

Based on the results of the experimental study, it was assumed that thermoelastic instability precedes thermomechanical failure (e.g., thermocracking), and that contact is concentrated at three (3) patches located at 120° from each other on the contact interface. It was also assumed that the patches are stationary with respect to the rotating mating ring, as was observed in our experimental program. The case of contact patches remaining stationary with respect to the carbon primary ring had been studied earlier [9,10]. The patches were estimated from microscopic observations of seal surfaces [9] to be about .1 to 1 mm long and dimensions in that range were used in this study.

It was assumed that each of the three contact patches encountered identical contact conditions, so only one 120° sector of the seal needed to be analyzed (see Figure 10). A finite element model of the shaft seal is shown in Figure 11. Overall dimensions and thermal boundary conditions were modelled after those of a typical marine shaft seal. The finite element mesh was two-dimensional (axial and circumferential directions), with variable thickness of the elements being used to account for heat flow in the radial direction. Elements as small as 10 μm xμ30 m were used in the contact zone, with elements as large as 24 mm x 15 mm used elsewhere in the mesh. The mesh used in the model contained 694 nodes and 644 elements.

For this model a uniformly distributed frictional heat source was assumed to be located at the contact interface. Convection boundary conditions were assumed to occur along the non-contacting portions of the seal interface, and fixed temperatures were applied to the boundary segments representing the back sides of the seal ring inserts. Material properties represented those of actual seal ring materials, and those properties were varied for the purpose of determining their influence on surface temperatures. Typical properties and boundary conditions are shown in Figure 11. A full parametric study, which involved variation of most of those properties, was performed to provide guidance for future seal material selection.

FINITE ELEMENT THERMAL ANALYSIS PROGRAM (THERMAP)

The finite element program used in this study was based on techniques developed earlier for studying surface temperatures in sliding systems [11]. The program has recently been modified and expanded, and its capabilities have been proven by comparison with closed form solutions for a variety of problems [15]. This new program, THERMAP, enables the transient, steady state, or quasi-steady state analysis of temperature distributions in moving or stationary bodies, or in systems composed of both moving and stationary components. In a transient analysis, boundary conditions, including convection, surface heat flux, or prescribed temperature may vary with time, as may velocity and internal heat generation rate. Material properties may be a function of temperature.

The equations on which THERMAP is based are developed in Appendix A. A flow chart for the program is presented in Appendix B, and user instructions for the program are in Appendix C.

The program's performance was verified by application to ten different problems for which closed-form solutions were available [15]. Each problem was designed to prove out a different capability of THERMAP. Excellent agreement was attained between theory and numerical prediction in all cases [15]. It was noted that numerical inaccuracies may occur in the solution of problems involving either high moving body velocities or excessively large time increments (for transient cases). The inaccuracies for both situations were characterized and criteria for their avoidance were developed [15]. Since the first of these two inaccuracies may occur in seal analyses, that problem was studied in some detail and a discussion of the problem and its solution follows later in this report.

One additional capability which was added to THERMAP so that systems like those in Figures 10 and 11 could be studied was "node tying." This procedure enables the equating of unspecified temperatures at any two (or more) nodes in the finite element mesh. For example, the seal shown in Figure 10 has three

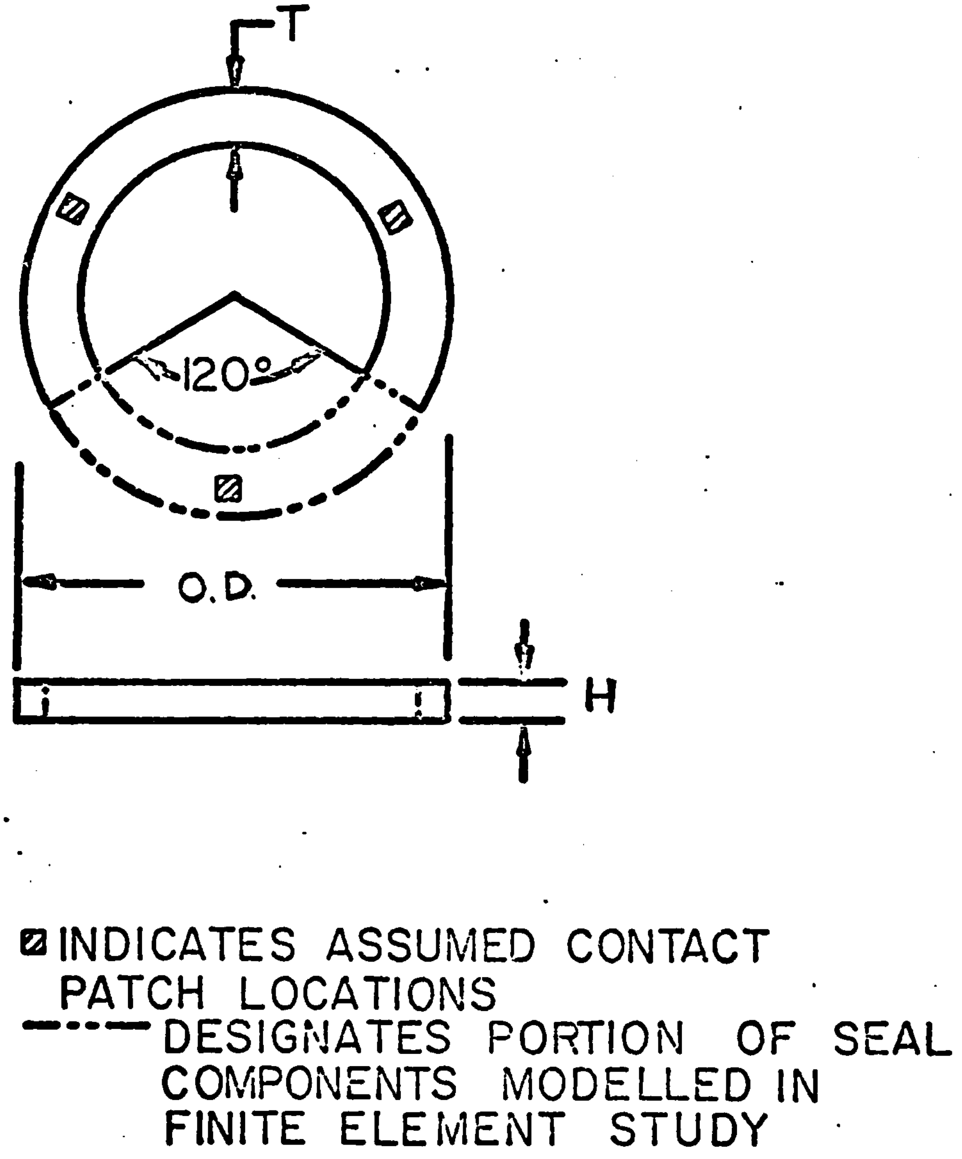
T
120°
O.D.
H
▨ INDICATES ASSUMED CONTACT PATCH LOCATIONS
—---— DESIGNATES PORTION OF SEAL COMPONENTS MODELLED IN FINITE ELEMENT STUDY

Figure 10. Sketch of primary seal ring, showing section studied in thermal and stress analyses.

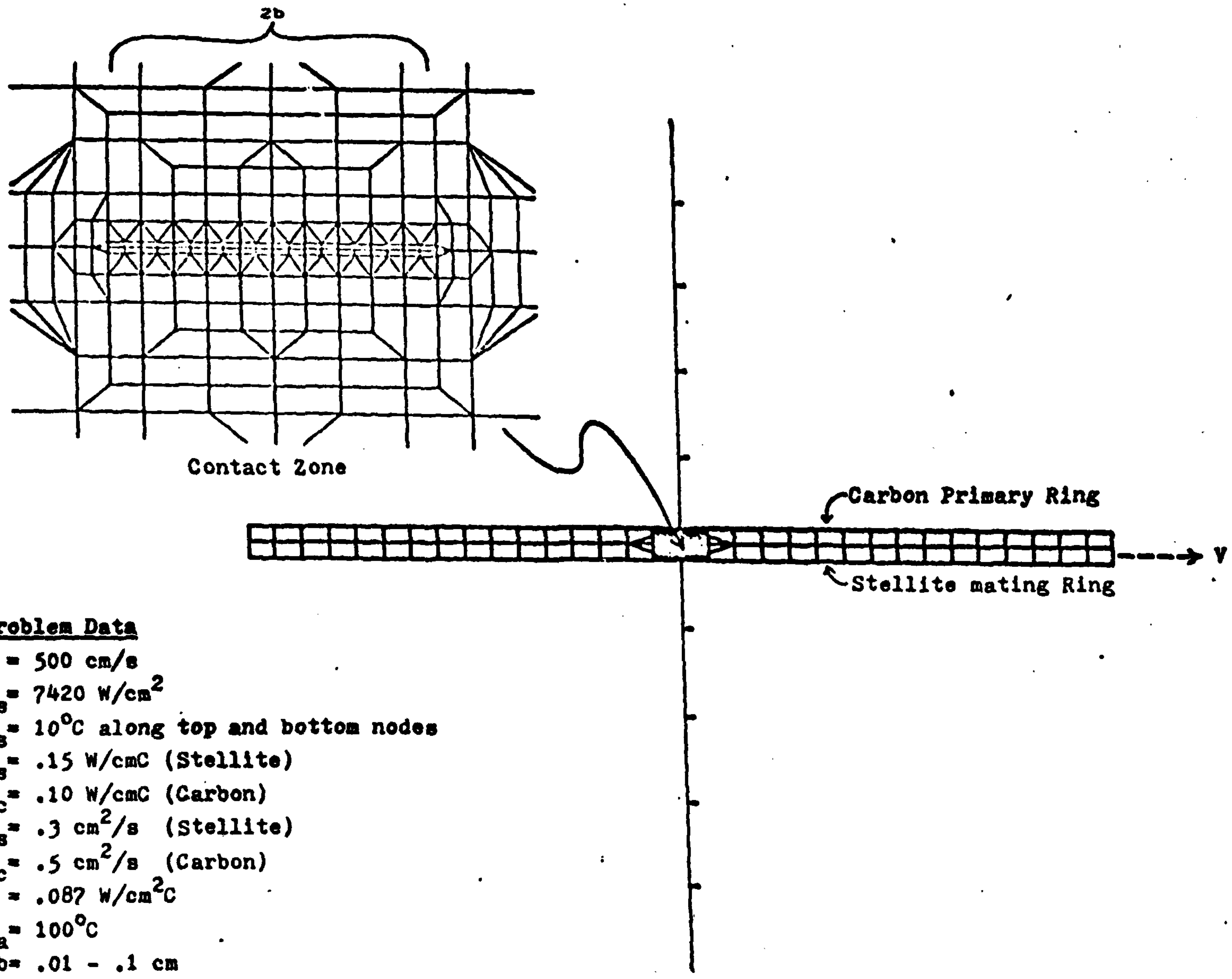
2b
Contact Zone
Carbon Primary Ring
Stellite mating Ring
V

Problem Data

$V = 500$ cm/s

$q_s = 7420$ W/cm^2

$T_s = 10^oC$ along top and bottom nodes

$K_s = .15$ W/cmC (Stellite)

$K_c = .10$ W/cmC (Carbon)

$\alpha_s = .3$ cm^2/s (Stellite)

$\alpha_c = .5$ cm^2/s (Carbon)

$h = .087$ W/cm^{2}C

$T_a = 100^oC$

$2b = .01 - .1$ cm

Fig. 11 . Finite Element Mesh for Mechanical Face Seal (V indicates that the stellite mating ring is moving relative to contact patch) contact patches on its surface. Each patch is considered identical, and the end of one 120° sector has the same temperature as the beginning of the next sector. The temperature distribution is, therefore, periodic in space. In order to analyze only one 120° sector, as in Figure 11, the nodes of one end of the seal sector must be "tied" to those at the other end so that the temperatures at the two ends will be equal.

FACTORS INFLUENCING SURFACE TEMPERATURES IN FACE SEALS

Using the THERMAP program described above, temperatures were calculated for the face seal model shown in Figure 11. A typical temperature distribution, calculated for a contact width 2b=.06 cm, had isotherms shown in Figure 12. In the figure the mating ring, which moves from left to right, is at the top, while the stationary primary ring is at the bottom. The contact patch is moving with the mating ring. It can be seen that the maximum surface temperature occurs near the rear (trailing edge) of the contact. Temperature gradients in the depth direction are greater in the primary ring, with respect to which the contact patch is moving. Much of the frictional heat is therefore being conducted into the primary ring. The high temperatures and high gradients in both seal rings lead to large thermal stresses which are predominantly compressive in nature. In the earlier phase of this project it was concluded that the large compressive stresses created near the hot patches induce localized plastic yielding on the mating ring seal face [9,10]. As the hot patches move to another spot on the seal face, owing to wear, the thermal stress is released and residual stresses occur in the plastically deformed region. It was hypothesized that these tensile residual stresses are responsible for thermocrack initiation [9,10].

To investigate the influence of the modelling assumptions and to observe the relative importance of the various material properties, a parametric study of all system variables was carried out. The results of 39 different calculations are shown in Table 3. From runs 1, 21, and 22 or 5 and 6, it can be seen that surface temperatures are approximately proportional to total frictional heat generation rate (= friction force x velocity). At a given heat generation rate, temperatures decrease with increasing velocity (runs 1-5), but the influence of velocity is not as strong as that of heat flux. Thus, at a constant friction force the temperature increases as the velocity increases (runs 1 and 6 or 3 and 22). This is in agreement with our experimental results (Table 2). One conclusion

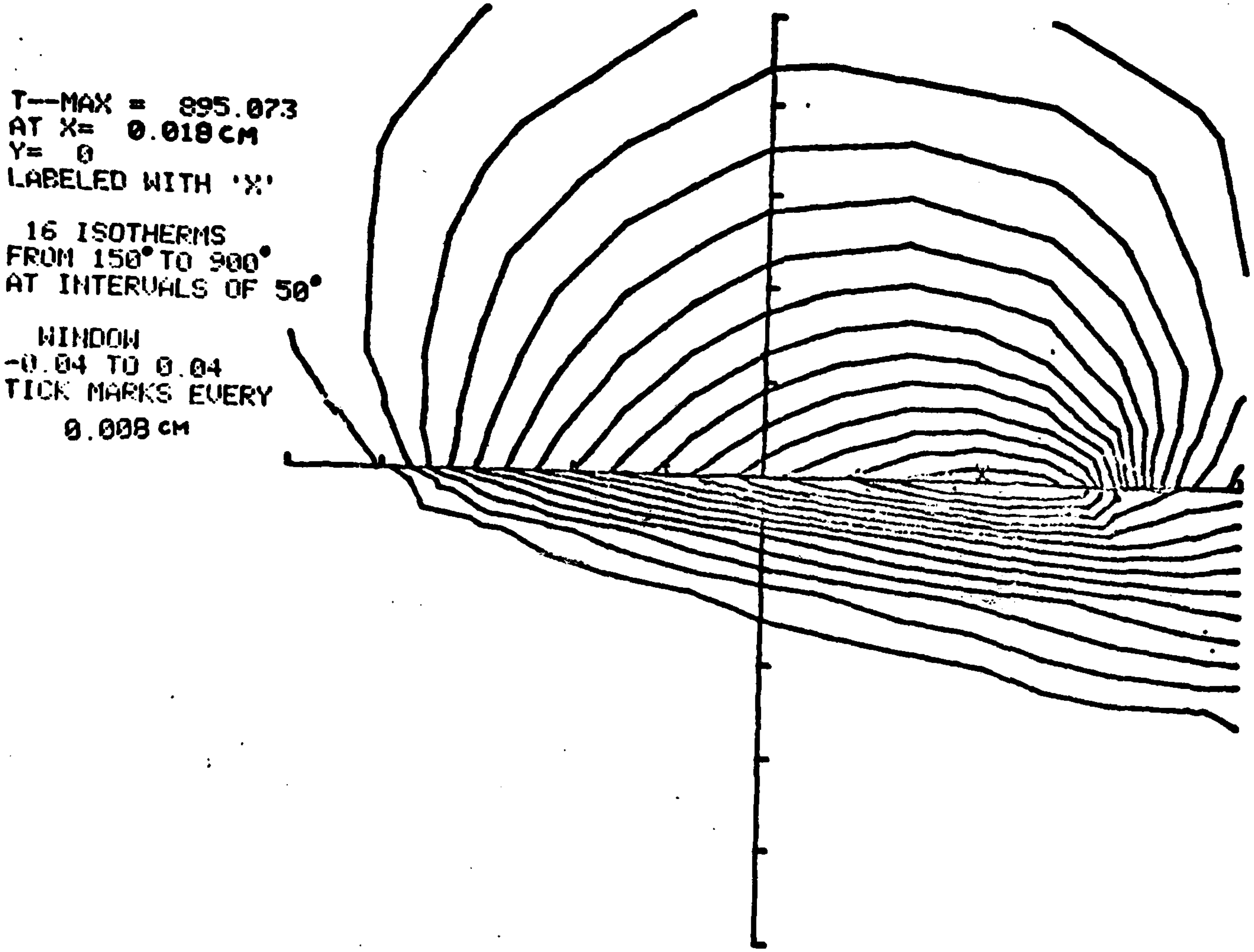

Figure 12. Isotherms in mating and primary seals for case of Figure 11.

of this study is that a reduction in seal velocity would reduce seal temperatures and, consequently, thermal stresses. This could be accomplished by a decrease of seal diameter.

The study showed that at a given heat generation rate and velocity, a reduction in contact patch size would result in higher patch temperatures (runs 23-27). This also agrees with our experimental results (Figure 9, for example). The influence of contact width on temperature is quite a bit smaller than that of total heat generation rate, so heat flux (heat generation/unit area) is less of a factor than total heat generation. Convective cooling was found to have a relatively small influence on surface temperature (runs 1, 18-20) with no significant cooling occurring until convection coefficient h becomes very high. Ambient temperature Ta has little influence over a reasonable range of values (runs 1, 15-17). Assumed prescribed temperature boundary conditions have a bit larger influence than convection so that bulk cooling could help lower surface temperatures. The change would not be dramatic, however (runs 1, 7-14).

Material properties, especially those of the primary seal ring, have a substantial influence on surface temperatures. An increase in thermal conductivity of the primary ring would cause a reduction in surface temperatures (runs 1, 33-35), while an increase in that material's thermal diffusivity, which normally accompanies an increase in conductivity, would have a lesser, but opposite, effect (runs 1, 36-39). The diffusivity of the mating ring material, on which the hot spot is stationary, has no effect on surface temperatures (runs 31-32), but the conductivity of that material is a significant factor (runs 1, 28-30). This dependence of surface temperatures on mating ring conductivity was also noted in our experimental study (Tables 1, 2). Considering these results, along with the interrelationship between thermal conductivity and thermal diffusivity, the best approach to reducing surface temperatures in seals might be to choose a higher conductivity mating ring material. An improvement in the primary ring conductivity would not be quite as effective unless the conductivity increase could be accomplished without a corresponding increase in diffusivity.

Run	V	Nodes	T_s	h	T_a	Heat	2b	K_m	α_m	K_p	α_p	T_{max}
1.	500cm/s	Top,Bot	10C	8.7W/cm^{2}C	100C	445 W	.06cm	15W/mC	.3cm^2/s	10W/mC	.5cm^2/s	613°C
2.	0											2597
3.	100											1034
4.	1000											489
5.	5000											315
6.	5000					4450						3031
7.	500		100			445						697
8.			0									603
9.		1	10									578
10.		1	100									657
11.		1,3	10									578
12.		2	10									636
13.		2	100									707
14.		2,4	10									637
15.		Top,Bot	10	8.7	0							606
16.				8.7	500							639
17.				8.7	1000							672
18.				0.0	100							618
19.				17.4	100							608
20.				870.0	100							549
21.				8.7	100	44.5	.06					76
22.						2225.0	.06					3000
23.						445.0	.048					660
24.						445.0	.032					732
25.						445.0	.024					846
26.						445.0	.012					1070
27.						445.0	.006					1288
28.						445.0	.06	3				700
29.								75				402
30.								1000				75
31.								15	.06			613
32.									1.50			613
33.									.3	2		1871
34.										50		150
35.										1000		17
36.										10	.1	372
37.											2.5	1034
38.											5.0	1274
39.											100.0	2301

TABLE 3. Parametric Study for Mechanical Face Seal Analysis
(Subscript p refers to properties of primary seal ring material
and subscript m refers to properties of mating ring material

EFFECT OF MOVING SURFACE VELOCITY ON THERMAL ANALYSIS

Evidence of Numerical Instabilities at High Velocity

The equations solved in the finite element analysis of surface temperature are derived from Fourier's law for heat conduction, equation (1) in Appendix A. At low surface velocities, the contribution of the term $V \cdot \nabla T$ in that equation is quite small, the governing differential is approximately parabolic, and the resulting finite element equations (equations (12) in Appendix A) are approximately symmetric. Few problems result in the solution of the equations and the results are quite accurate as long as the mesh is fine enough to model temperature gradients and the time increment is small enough to follow transient changes [15]. When the velocity is large, however, the first derivative terms become significant, the governing equation is to some extent hyperbolic, and the resulting finite element equations are nonsymmetric. It has been found by numerous investigators in recent years [e.g., 18], that numerical oscillations may develop in the solution of equations similar to these at high velocities. Such equations, often called convective-diffusion equations because of the presence of the convective or advective term $V \cdot \nabla T$, appear in a variety of transport problems, and numerical oscillations are encountered in both finite difference and finite element solutions of the equations in fluid flow and heat transfer investigations.

In order to study the magnitude of the problem, a simple sliding contact problem (metallic slider on metallic flat) was analyzed under quasi-steady state conditions using the finite element model shown in Figure 13a on the left. A blowup of the mesh at the contact zone is shown in Figure 13a on the right. Heat generation due to friction was modeled by a uniform heat flux within the contact zone. A fixed temperature of 22°C was set at the lower left corner of the mesh. Figures 20b - 20c show the isotherms predicted by THERMAP for values of velocity ranging from V=0 to V=100,000 cm/s. Isotherms are plotted both in the complete mesh and in the contact region at regular intervals of ΔT. The isotherms drawn in Figures 20b - 20e seem quite reasonable in both sliding and stationary bodies. For these low velocities the isotherms and temperature magnitudes are affected by velocity, but no solution difficulties were encountered. When the velocity reaches 50 cm/s for this problem, however, spatial oscillations begin to appear in the moving body temperature field and at slightly higher velocities (Figs. 20g-20k) the surface temperature predictions are definitely inaccurate. At even higher velocities (Figure 20ℓ-20m) the temperature magnitudes seem reasonable, but spatial oscillations reappear in the moving body. Thus it became apparent that the application of THERMAP to problems of high sliding velocity could lead to invalid temperature predictions.

To study the problem in more detail, another sample problem was posed. In this problem, the model of which is shown in Figure 14a, a uniformly distributed heat flux q was applied to a band on the surface of a moving, two-dimensional slab. Temperatures in the body were analyzed for a variety of different conditions and the results of some of the runs are given in Table 4.

A study of the data in Table 4 shows that oscillations may occur whenever the velocity of the moving body relative to the heat source reaches a critical value. That critical value is a function of the diffusivity of the material of that body and of the size of the finite elements. In particular, it appears that oscillations occur whenever the element Peclet number is equal to or greater than 2,

$$P_e = \frac{V\Delta x}{D} \geq 2 \qquad (1)$$

The critical Peclet number appears to be applicable to the largest element in a region where there are significant temperature gradients. In runs 18-20, for example, it was found that oscillations first began, not at the heat source, but a slight distance away where the elements were larger (and P_e was larger). If the velocity continues to increase, oscillations could move into regions where the elements are smaller when the critical Peclet number for those elements is reached. This critical value of 2 for the element Peclet number is the same number determined by other researchers [19] for analysis of convective diffusion equations using linear elements. That study also showed that the critical

Figure 13. Study of Velocity effect in frictionally heat generating contact problem. (System shown on left, contact zone on rt)

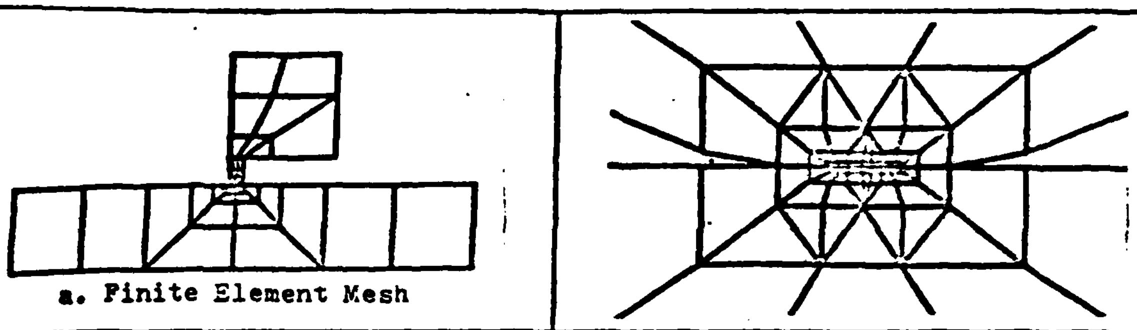

a. Finite Element Mesh

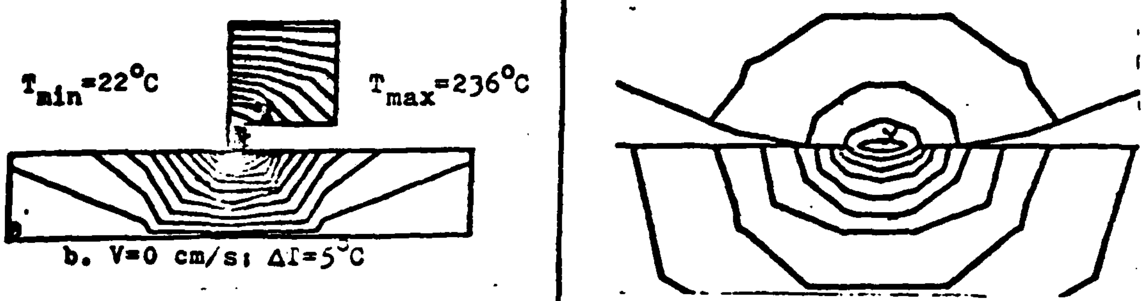

b. V=0 cm/s; ΔT=5°C

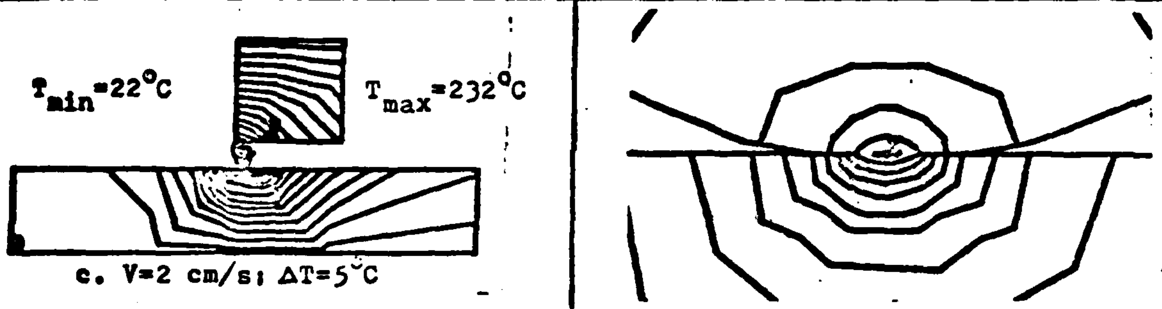

c. V=2 cm/s; ΔT=5°C

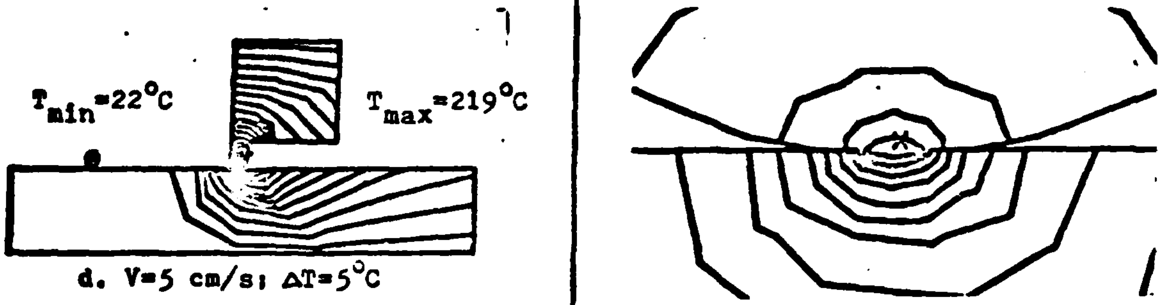

d. V=5 cm/s; ΔT=5°C

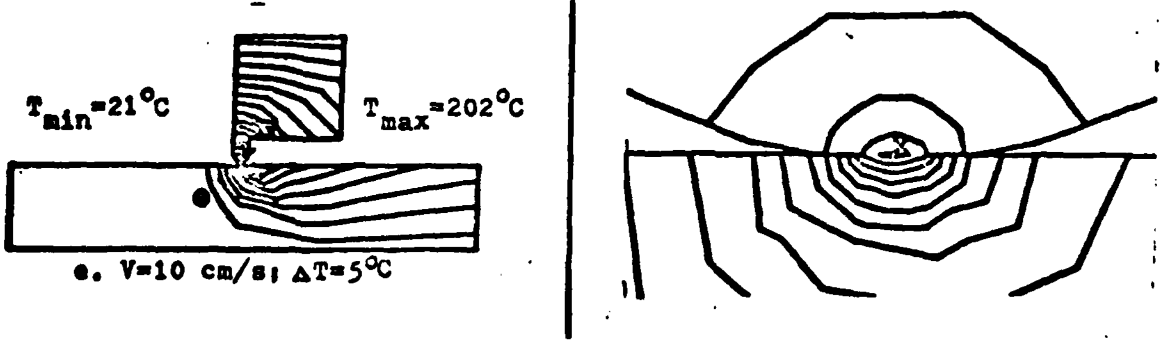

e. V=10 cm/s; ΔT=5°C

Figure 13 (continued)

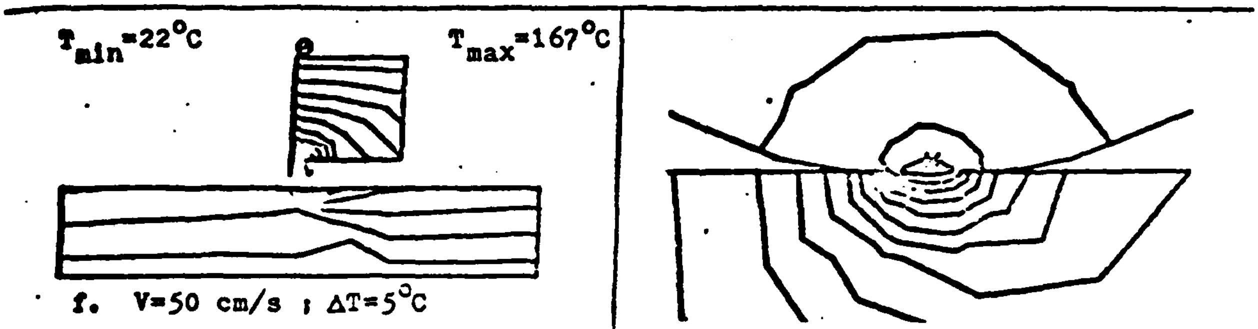
T_{min}=22°C
T_{max}=167°C

f. V=50 cm/s ; ΔT=5°C

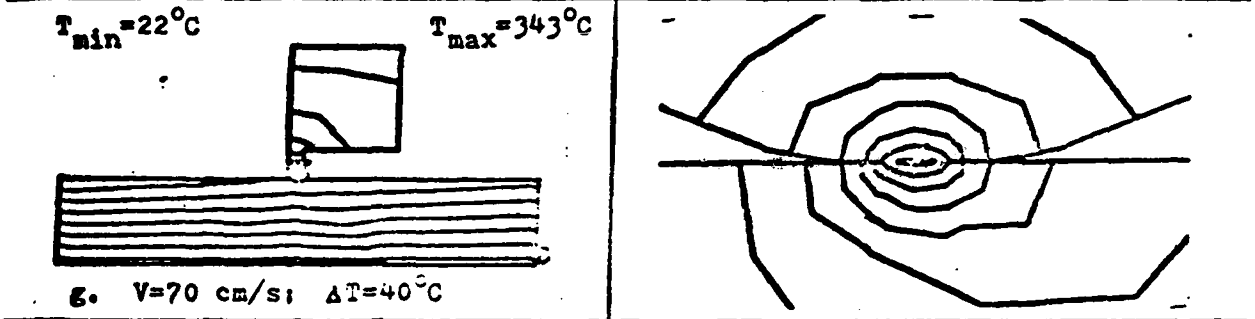
T_{min}=22°C
T_{max}=343°C

g. V=70 cm/s; ΔT=40°C

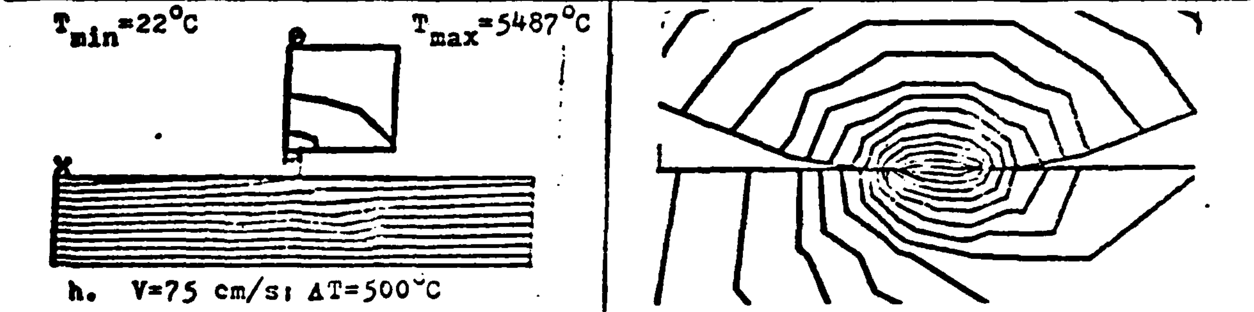
T_{min}=22°C
T_{max}=5487°C

h. V=75 cm/s; ΔT=500°C

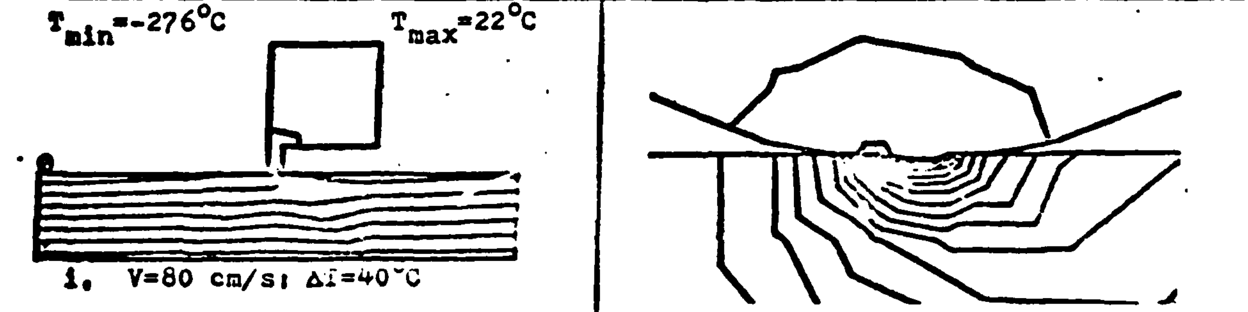
T_{min}=-276°C
T_{max}=22°C

i. V=80 cm/s; ΔT=40°C

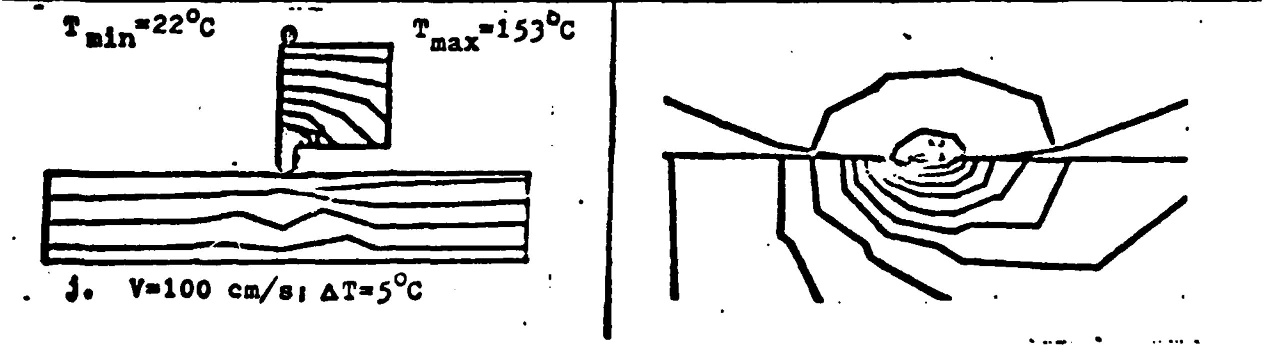
T_{min}=22°C
T_{max}=153°C

j. V=100 cm/s; ΔT=5°C

Figure 13 (continued)

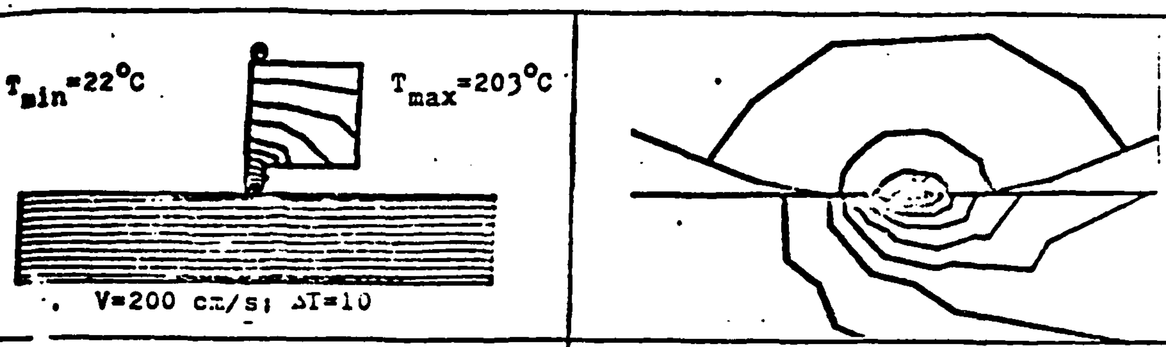
T_{min}=22°C
T_{max}=203°C

V=200 cm/s; ΔT=10

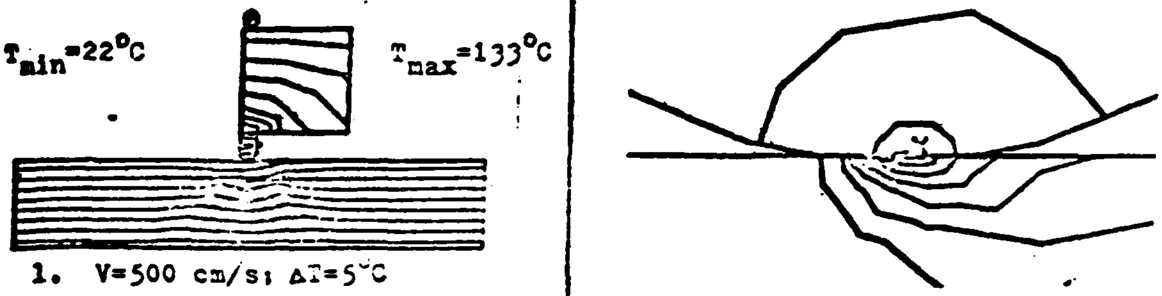
T_{min}=22°C
T_{max}=133°C

l. V=500 cm/s; ΔT=5°C

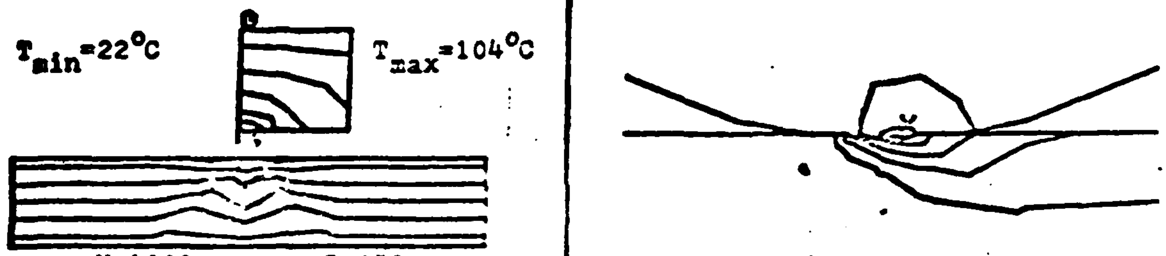
T_{min}=22°C
T_{max}=104°C

m. V=1000 cm/s; ΔT=5°C

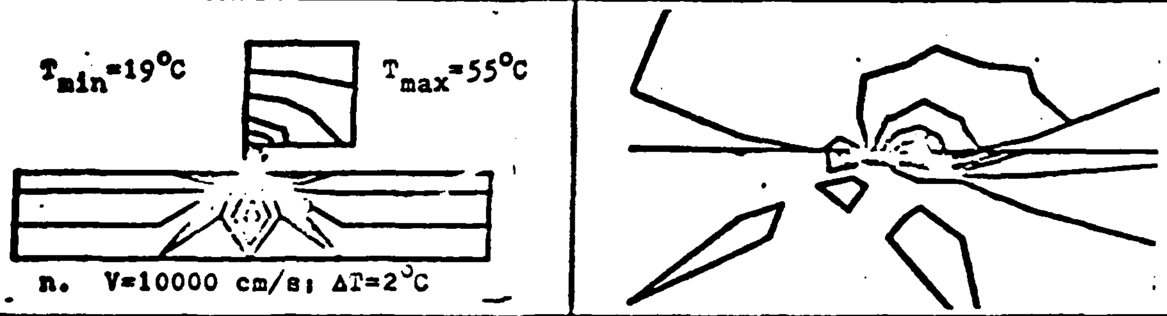
T_{min}=19°C
T_{max}=55°C

n. V=10000 cm/s; ΔT=2°C

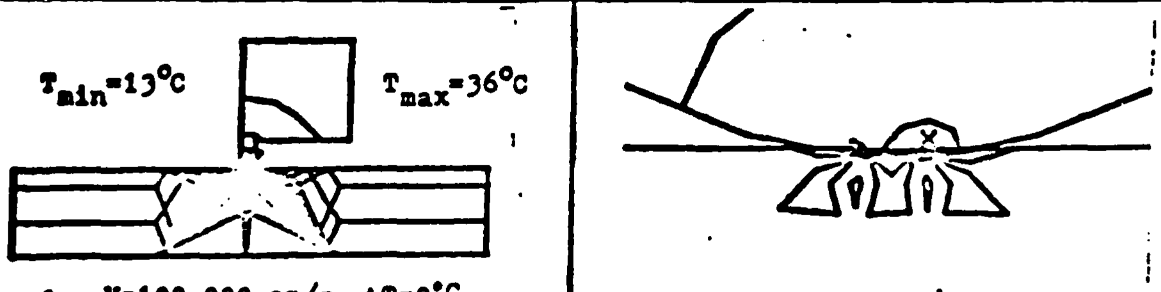
T_{min}=13°C
T_{max}=36°C

o. V=100,000 cm/s; ΔT=2°C

value may be slightly different for different element interpolation functions [19]. The results of our study (e.g., run 11) also show that the critical Peclet number value may be even lower than 2 if the temperature gradients within the elements are large, owing to high heat flux, for example.

It can also be seen that results at Peclet numbers above the critical value may not be too inaccurate unless the oscillations are occurring in the region of interest, usually the heat flux zone. As was the case in the earlier study (Figure 13) at Peclet numbers much higher than 2, Run 17 for example, the results can be quite reasonable and relatively oscillation-free. The worst results seem to occur at Peclet numbers between 4 and 40. There are a great many potential applications in that region. In such cases, the problem of numerical oscillations and inaccuracies could be a serious deterrent to the use of finite element thermal analysis programs like THERMAP in surface temperature analysis.

There are two possible remedies to this problem. The simplest is to make the finite element mesh smaller, at least in the region where numerical oscillations are occurring. This, in fact, may be the best solution in many cases because it may enable more accurate representation of temperature gradients in the region of interest. A large reduction in mesh size may, however, lead to an excessive increase in computer time and memory requirements. An alternative is to modify the numerical procedure in order to avoid solution oscillations. This approach has been the focus of intensive study recently.

Techniques for Handling Convective-Diffusion Equations

The problem of numerical oscillations at high Peclet number occurs in both finite element and finite difference solution of equations of the convective-diffusion type. Such equations occur in a variety of transport problems, including fluid flow, seepage, and heat conduction. Because of this, numerous investigators have been attempting in recent years to find ways to overcome the oscillation problems. In this work we are most concerned with techniques for

TABLE 4

Results of Thermal Analysis of Moving Slab Subject to Distributed Heat Source

Run	Heat Flux q	ΔX_1	ΔX_2	Diffusivity D	Velocity V	$\frac{V\Delta X_1}{D}$	T_{max}	Comments
1	100	.1	.1	1	10	1	111.5	good results
2	100	.1	.1	1	20	2	108.2	slight subsurface oscillations
3	100	.1	.1	1	40	4	106.0	oscillations on and beneath surface
4	100	.1	.1	.667	10	1.5	114.1	good results
5	100	.1	.1	.5	10	2	116.4	slight subsurface oscillations
6	100	.1	.1	.25	10	4	124.1	oscillations on and beneath surface
7	100	.05	.05	1	35	1.75	104.4	good results
8	100	.05	.05	1	40	2	104.1	beginnings of subsurface oscillations
9	100	.05	.05	1	50	2.5	103.7	subsurface oscillations
10	1000	.05	.05	1	30	1.5	147.0	good results
11	1000	.05	.05	1	35	1.75	143.5	beginnings of subsurface oscillations
12	1000	.05	.05	1	40	2	140.9	subsurface oscillations
13	1000	.05	.05	1	100	5	127.1	oscillations under contact
14	1000	.05	.05	1	200	10	120.3	slight oscillations under contact
15	1000	.05	.05	1	400	20	119.7	no subsurface oscil., slight surf.rippl
16	1000	.05	.05	1	800	40	120.9	no subsurface oscil., ripple on surface
17	1000	.05	.05	1	1600	80	119.2	" " " " " "
18	1000	.1	.05	1	20	2	156.5	oscillation just beginning(in ΔX_1 regio
19	1000	.1	.05	1	25	2.5	150.9	slight oscil. in ΔX_1 region
20	1000	.1	.05	1	30	3	146.6	oscil. beginning to touch ΔX_2 region
21	1000	.1	.05	1	40	4	140.3	oscillations under contact (ΔX_2 region)

Figure 14

Finite Element Test Models for Study of Velocity Effect

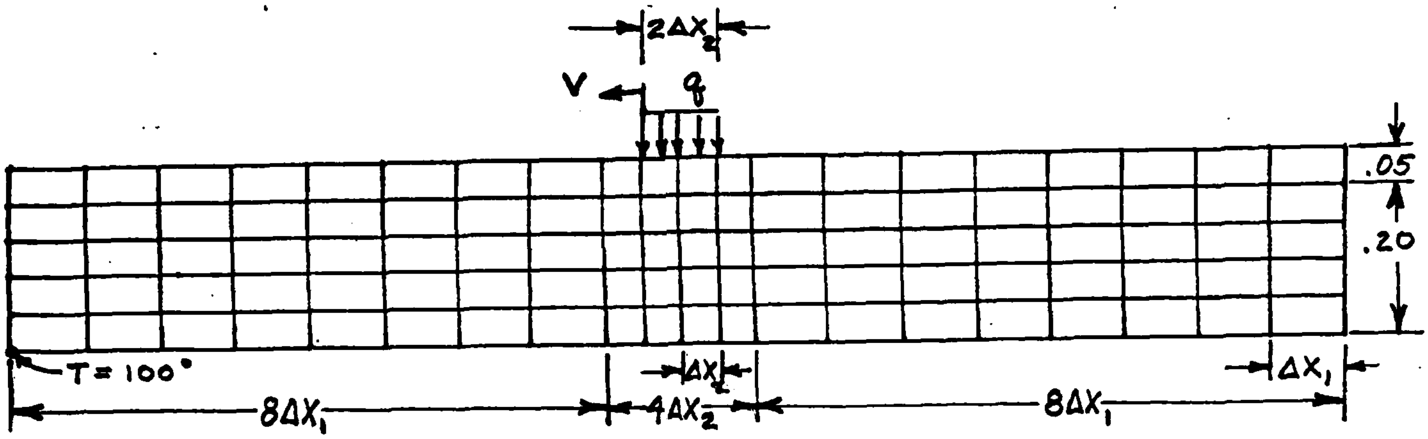
2ΔX₂
V
q
.05
.20
T = 100°
ΔX₂
ΔX₁
8ΔX₁
4ΔX₂
8ΔX₁

(a) 2-Dimensional Model (Moving Slab)
Heat Flux q moving at Velocity V relative to slab

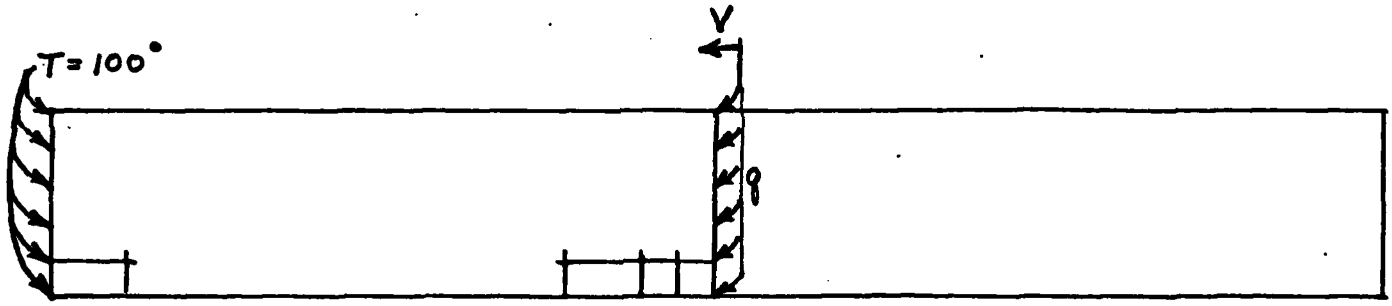

(b) 1-Dimensional Model (Moving Rod)
Heat Flux q moving at Velocity V relative to Rod
Same mesh dimensions as in (a)

use with finite element methods and, for the moment, in two-dimensional studies with bilinear finite elements.

A variety of techniques have been developed for use in this type of situation in the past few years. Among them are the following:

1. The method of Finn and Varoglu [20], which employs space-time finite elements and incorporates the characteristics of the hyperbolic portion of the partial differential equation.

2. A method developed by O'Neill and Lynch [21], in which the heat conduction equations are formulated in terms of a moving coordinate system. Although the convection or advection term is absent in such a formulation, the finite element mesh must be continuously deforming.

3. A procedure recently proposed by Kanarochos [22], in which the conventional Galerkin finite element equations (eqns. 12 in Appendix A), are solved, but special boundary-layer type elements are used in that portion of the moving body in which the temperature gradients are significant.

4. Upwinding finite element schemes, used by Neinrich et.al. [23], and others. In that technique the finite element equations are developed using a weighted residual method with a weighting function. W_i different from the interpolation functions N_i. The weighting functions used by Heinrich, et. al. [23], were of the form $W_i = N_i + \alpha F_i$ where α is a function of the element Peclet number.

5.The streamline upwind formulation developed by Brooks and Hughes [25], in which the weighting functions (see #4 above) are constants which act only in the velocity direction.

6. A different type of upwinding developed by Baliga and Patankar [24], in which both weighting function and interpolation function vary with Peclet number. In their formulation the functions vary exponentially in the velocity direction, but become equal to the linear interpolation functions N_i when the velocity decreases to zero.

A study of each of these techniques and their applicability to heat conduction problems with moving heat sources revealed that the upwinding techniques are the easiest of the above procedures to implement and possibly the most suitable for this application. Two of the techniques (#5 and 6) were implemented in THERMAP.

Application of upwinding technique to THERMAP

In the original formulation of the finite element equations in THERMAP (see Appendix A), the Galerkin procedure was employed with weighting functions Ni, which are also the interpolation functions used in the approximation of the temperature across an element. For the linear triangle element, the interpolation functions are given by [16]:

$$N_i = \frac{1}{2} \left[(X_j Y_k - X_k Y_j) + X(Y_j - Y_k) + Y(X_k - Y_j) \right] \qquad (2)$$

where (X_i, Y_i), (X_j, Y_j), and (X_k, Y_k) are the coordinates of the of the element's three corner nodes and Δ is the area of the element.

In our version of the Brooks-Hughes technique, the interpolation functions remain the same but the weighting functions become:

$$W_i = N_i + \bar{k} \left(V_x \frac{\partial N_i}{\partial X} + V_y \frac{\partial N_i}{\partial y} \right) / V^2 \qquad (3)$$

where V_x and V_y are the x and y components of velocity

$V^2 = V_x^2 + V_y^2$

and $\bar{k}$ is a constant which depends on the element Peclet number [25]

TABLE 5

Results of One-Dimensional Thermal Analysis with Moving Heat Source

Run	ΔX_1	ΔX_2	D	V	$\frac{V\Delta X_1}{D}$	T_{55}	T_{55} Theory	Upwinding	Comments
1	.05	.05	1	1	.05	103.48	103.46	none	good results
2	.05	.05	.025	1	2	100.0	101.35	"	slight ripple near source
3	.05	.05	.05	2	2	100.0	100.68	"	slight ripple near source
4	.1	.05	.02	1	5	98.89	100.82	"	oscillation near source
5	.1	.1	.04	1	2.5	98.89	100.82	"	oscillation near sourse
6	.1	.05	1	1	.1	105.47	105.47	Baliga	good results
7	.1	.05	.02	1	5	100.81	100.82	"	" "
8	.1	.05	.01	1	.1	99.73	100.07	"	slight osc. near source
9	.1	.05	1	1	.1	105.47	105.47	Brooks	good results
10	.1	.05	.01	1	10	100.07	100.07	"	" "
11	.1	.05	.0001	1	1000	100.00	100.00	"	" "

TABLE 6

Moving Slab with Distributed Heat Source
- Results of Analysis with Upwinding

Velocity V	$\frac{V X_i}{D}$	Temperature at Node 66 ($\approx T_{max}$)		
		No Upwinding	Baliga	Brooks
0	0	605.39	605.26	605.39
.001	.0001	604.91	604.94	604.91
.01	.001	602.64	602.61	602.64
.1	.01	580.73	580.58	580.68
1	.1	421.51	421.48	421.38
10	1	180.05	179.91	179.84
20	2	156.5 *	156.77	156.53
40	4	140.3 **	140.5 *	139.85
100	10	123.21 **	125.34 **	123.37
1000	100	-	-	104.37 *

* Oscillations just about beginning.
** Oscillations in solution.

When these weighting functions are used in a weighted residual procedure (the Petron-Galerkin procedure), finite element equations are obtained which are identical to those given in Appendix A except for a modified Kv_{ij} term (in equation 3, Appendix A). The modified term reduces to the Kv_{ij} given in Appendix A for the case of zero velocity. For non-zero velocities, the inclusion of Pi weights the resulting stiffness matrix contribution in the direction of positive velocity.

In the Baliga-Patankar method, the weighting function is set equal to the interpolation function, but both are different from the relations given in eqn. (2). A new coordinate system X,Y is defined in the x,y plane with the X axis oriented in the velocity direction. A new variable Z is defined [24] such that:

$$Z = \frac{D}{V} \quad \exp\left[\frac{V}{D}(X - Xmax) - 1\right] \qquad (4)$$

where D is the material's diffusivity

and Xmax is the maximum (most positive) X coordinate location of the element's nodes.

Using this, the interpolation function becomes:

$$N_{i_B} = \frac{1}{2\Delta_Z}\left[(Z_j Y_k - Z_k Y_j) + Z(Y_j - Y_k) + Y(Z_k - Z_j)\right] \qquad (5)$$

where Z_i, Z_j, Z_k are the Z values at the element's nodes

and Δ_Z is the area of the triangle formed by (Z_1, Y_1), $(Z_2 m\ Y_2)$, (Z_3, Y_3)

This interpolation function is then used in eqn. (3) of Appendix A to get the finite element equations for this formulation. Because of the non-linear nature of Z, the integrals for each element must be evaluated numerically.

Modified versions of THERMAP were written to include the above modifications in the finite element equations. The programs, along with the original version, were applied to the two test problems shown in Figure 14. One of the problems is the same 2-dimensional problem studied earlier (Table 4), while the other is a problem involving 1-dimensional heat flow in a moving rod (Figure 14b). The results of some of the tests are presented in Tables 5 and 6.

In Table 5 the predictions of the original version of THERMAP are compared with those of the Brooks-Hughes and Baliga-Patankar versions. Also included are analytical predictions from a closed form solution available for this case [26]. All three versions of the program gave good predictions for element Peclet numbers less than 2, in accordance with equation (1). When the Peclet number of the largest element in the mesh reached or exceeded 2, however, oscillations began to appear in the numerical results using the original THERMAP version. The oscillations were accompanied by inaccuracies in the temperature predictions for nodes just ahead of the heat source. The oscillations and inaccuracies occurred whether the Peclet number was increased by an increase in element size, an increase in velocity, or a decrease in diffusivity. The Baliga-Patankar version gave good predictions for element Peclet numbers less than about 8, a four-fold improvement over the original version. At higher Peclet numbers, however, the results deteriorated, producing the same type of inaccuracies and oscillations noted at lower Peclet numbers with the original version (e.g., Run 8). The Brooks-Hughes version, on the other hand, gave good predictions over the entire range of Peclet numbers from 0 to 10,000. No oscillations were noted in any of the solutions with that technique and all results agreed well with theoretical predictions.

Results for the two dimensional problem (Fig. 14a) are given in Table 6. Results are somewhat less satisfying than for the one-dimensional heat flow problem. As was seen earlier, the original version of THERMAP produced good results for element Peclet numbers less than 2. With the Baliga-Patankar version, oscillation-free results continued until Peclet number reached 4 but oscillations occurred in solutions at higher Peclet numbers. Again the Brooks-Hughes method gave the best results, with oscillations not beginning until the largest element Peclet number reached about 60. Some oscillations occurred at higher Peclet numbers, but in all cases they were less severe than those found with the other techniques at the same Peclet number. Slight differences were noted between the predictions of the different programs, but the differences were not great. No closed-form solution exists with which to compare the predictions.

CONCLUSIONS FROM ANALYTICAL STUDY

The finite element surface temperature analysis program THERMAP, developed and used in this study, has proven to give good predictions of seal temperature distributions for a wide variety of conditions. Use of the program in a parametric study showed that seal surface temperature is approximately proportioned to total heat generation rate (= fixation force X seal surface velocity). A reduction in seal velocity, by a reduction in seal diameter, would result in a temperature decrease. Smaller decreases in temperature could be accomplished by an increase in convective cooling or by bulk cooling of the seal rings. Material properties of the seal rings were found to have a significant influence on seal surface temperatures, with higher thermal conductivity of both primary and mating seal rings leading to substantial decreases in temperatures. If the increase in primary seal ring conductivity is accompanied by a corresponding increase in that material's diffusivity, however, much of the decrease in surface temperature would be wiped out.

The thermal analysis showed that numerical oscillations and inaccuracies can occur if the element Peclet number of the primary seal model exceeds 2 in the vicinity of significant temperature gradients. This can occur with either high surface velocities, low thermal diffusivity, or large element sizes. The problem is similar to that encountered by other researchers in recent years with equations of the convective-diffusion type. Several methods were studies as a means to avoid the numerical oscillations and it was found that the streamline upward procedure developed by Brooks and Hughes leads to a substantial improvement in the solution at high Peclet numbers without excessive computing effort. That procedure has now been incorporated in THERMAP.

REFERENCES

1. Abar, J.W., "Rubbing Contact Materials for Face-Type Mechanical Seals", Lubrication Engineering, 20 (1964), 381-386.

2. Golubien, A.I., "Thermocracking of Seal Faces in Mechanical Seals", Proc. 5th Int. Conf. on Fluid Sealing, Warwick, England, 1971, A2-9 to A2-16.

3. Lebeck, A.O., "Mechanical Loading-A Primary Source of Waviness in Mechanical Face Seals", ASLE Transactions, 20 (1977), 195-208.

4. Burton, R.A., Nerlikar, V., and Kilaparti, S.R., "Thermoelastic Instability in a Seal-Like Configuration", Wear, 24 (1973), 177-188.

5. Kilaparti, R., and Burton, R.A., "A Moving Hot Spot Configuration for a Seal-Like eometry, with Frictional Heating, Expansion, and Wear", ASLE Transactions, 20 (1977, 64-70.

6. Burton, R.A., "Thermal Deformation in Frictionally Heated Contact", Wear, 59 (1980), 1-20.

7. Lebeck, A.O., "Theory of Thermoelastic Instability of Rotating Rings in Sliding Contact with Wear", ASME J. of Lubrication Technology, 98 (1976), 277-285.

8. Netzel, J.P., "Observation of Thermaelastic Instability in Mechanical Face Seals", Wear, 59 (1980), 135-148.

9. Kennedy, F.E. and Karpe, S.L., "Thermocracking of a Mechanical Face Seal", Wear, 79 (1982), 21-36.

10. Kennedy, F.E., Grim, J.N., and Glovsky, R.P., "Factors Influencing Thermomechanical Failure of Face Seals", Interim Report #1 submitted to ONR, Thayer School of Engineering, January 1982.

11. Kennedy, F.E., "Surface Temperatures in Sliding Systems - A Finite Element Analysis", ASME J. of Lub. Tech., 103 (1981), 90-96.

12. Dow, T.A. and Stockwell, R.D., "Experimental Verification of Thermoelastic Instabilities in Sliding Contact", ASME J. of Lub. Technology, 99 (1977), 359-364.

13. Bannerjee, B.N. and Burton, R.A., "Experimental Studies of Thermoelastic Effects in Hydrodynamically Lubricated Face Seals", ASME J. of Lub. Tech., 101 (1979), 275-282.

14. Grim, J.N., "Observation of Thermoelastic Instabilities in Mechanical Face Seals", Master of Engineering Thesis, Thayer School of Engineering, July 1982.

15. Glovsky, R.P., "Development and Application of THERMAP", Master of Engineering Thesis, Thayer School of Engineering, June 1982.

16. Huebner, K.H., The Finite Element Method for Engineers, Wiley, New York, 1975.

17. Bathe, K., and Wilson, E.L., Numerical Methods in Finite Element Analysis, Prentice-Hall, Inc., Englewood, N.J., 1976.

18. Hughes, T.J.R., Editor, "Finite Element Methods in Convection Dominated Flows", AMD Vol. 34, ASME, New York, 1979.

19. Jensen, O.K., and Finlayson, B.A., "Oscillation Methods for Weighted Residual Methods Applied to Convective Diffusion Equations", Int. J. Num. Meth. Eng., 15 (1980), 1681-1689.

20. Finn, W.D.L. and, Varioglu, E., "A Characteristics Based Finite Element Method for Heat Transport Problems", in Numerical Methods in Heat Transfer, edited by R.L. Lewis et al, Wiley & Sons, New York, 1981, 373-385.

21. O'Neill, K. and Lynch, D., "Efficient and Highly Accurate Solution of Diffusion and Convective-Diffusion Problems, using Moving, Deformable Coordinates, in Finite Elements in Water Resources, III, edited by Wang, et al., 1981.

22. Kanarachos, A., "Boundary Layer Refinements in Convective Diffusion Problems", Int. J. for Num. Meth. Eng., 18 (1982), 167-180.

23. Heinrich, J.C., Huyakorn, P.S., Zienkiewicz, O.C., and Mitchell, A.R., "An 'Upwind' Finite Element Scheme for Two-Dimensional Convective Transport Equation", Int. J. Num. Meth. Engg., 11 (1977), 131-143.

24. Baliga, B.R., and Patankar, S.V., "A New Finite Element Formulation for Convective Diffusion Problems", Numerical Heat Transfer, 3 (1980), 393-409.

25. Brooks, A.N. and Hughes, T.J.R., "Streamline Upwind/Petrov-Galerkin Formulations for Convective Dominated Flows", Computer Methods in Appl. Mech. & Engg., 32 (1982), 199-259.

26. Carslaw, H.S., and Jaeger, J.C., Conduction of Heat in Solids, 2nd Ed., Clarendon Press, Oxford, 1959.

APPENDIX A

THEORETICAL DEVELOPMENT OF EQUATIONS [15]

Consider Fourier's law for heat conduction in an anisotropic solid moving with velocity V:

$$\nabla \cdot K\nabla T + Q - \rho C(\partial T/\partial t) - V \cdot \nabla T = 0 \qquad (1)$$

Kennedy[11] developed the finite element equations for the quasi-stationary condition, $(\partial T/\partial t) = 0$, reducing equation (1) to:

$$\nabla \cdot K\nabla T + Q - V \cdot \nabla T = 0 \qquad (2)$$

The temperature solution must satisfy the following boundary conditions:

$T = Ts$ prescribed temperature in specified regions, S1
$qs \cdot n = K\nabla T \cdot n$ prescribed heat flux normal to surface, S2
$h(Ta-T) \cdot n = K\nabla T \cdot n$ convection to Ta across surface, S2

The continuum being modeled is discretized into finite elements with a temperature, Ti, being associated at each vertex (node). Assuming that the temperature field is linearly distributed throughout each element temperature is defined:

$$T = \sum_{i=1}^{m} NiTi^{e} = [N]^{e}\{T\}^{e}$$

where m is the total number of nodes in an element and Ni are the interpolation functions[16]. Applying the Galerkin method[16] and integrating the resulting equation by parts, Kennedy[11] arrives at the finite element equations in matrix notation:

$$([Kt]+[Kh]+[Kv])\ \{T\} = \{Q\}+\{q\}+\{KTa\} \qquad (3)$$

where:

$$Kt_{ij} = \int_{D^e} d[Kx(\partial Ni/\partial x)(\partial Nj/\partial x) + Ky(\partial Ni/\partial y)(\partial Nj/\partial y)]dxdy$$

$$Kh_{ij} = \int_{S^e} hNiNjdS$$

$$Kv_{ij} = \rho C \int_{D^e} dNi[Vx(\partial Nj/\partial x) + Vy(\partial Nj/\partial y)]dxdy$$

$$Q_i = \int_{D^e} dQNidxdy$$

$$q_i = \int_{S^e} qsNidS$$

$$KTa_i = \int_{S^e} hTaNidS$$

for 2-dimensional heat flow in the xy plane.

To solve 3-dimensinal axisymmetric systems (i.e. 2-dimensional heat flow in the rz plane), the matrix notation is redefined:

$$Kt_{ij} = 2\pi \int_{D^e} r[Kr(\partial Ni/\partial r)(\partial Nj/\partial r) + Kz(\partial Ni/\partial z)(\partial Nj/\partial z)]drdz$$

$$Kh_{ij} = \int_{S^e} hNiNjdS$$

$$Kv_{ij} = 2\pi\rho C\int_{D^e} rNi[Vr(\partial Nj/\partial r) + Vz(\partial Nj/\partial z)]drdz$$

$$Q_i = 2\pi\int_{D^e} rQNidrdz$$

$$q_i = \int_{S^e} qsNidS$$

$$KTa_i = \int_{S^e} hTaNidS$$

Noté that the integral over the element surface, Se, will take on different values depending on whether the problem is 2-dimensional or 3-D axisymmetric.

For simplicity equation (3) may be rewritten:

$$[S]\{T\} = \{R\} \qquad (4)$$

where $[S] = [Kt]+[Kh]+[Kv]$ and
$\{R\} = \{Q\}+\{q\}+\{KTa\}$.

The desired temperature distribution is arrived at by solving for $\{T\}$ in equation (4).

To modify THERMAP for handling transient thermal analyses, the finite element equations must be derived from equation (1) instead of equation (2). This modification changes equation (4) to:

$$[S]\{T\} + [C]\{\dot{T}\} = \{R\} \qquad (5)$$

where $[C] = \rho C \int_{D^e} dNiNjdxdy$ for 2-D flow in xy plane or

$$[C] = 2\pi\rho C \int_{D^e} rNiNjdrdz$$ for 2-D axisymmetric flow in rz plane.

Equation (5) differs from equation (4) by the addition of the time derivative term, $[C]\{\dot{T}\}$.

To facilitate solving equation (5) by computer, the following finite difference time stepping scheme[17] is used:

$$\{T\}_t = \{T\}_{t-\Delta t} + \Delta t(\theta\{\dot{T}\}_t + (1-\theta)\{\dot{T}\}_{t-\Delta t}) \qquad (6)$$

For $\theta=.5$, equation (6) reduces to the Crank-Nicholson[17] approximation.

Rearrange equation (6) to solve for $\{\dot{T}\}_t$:

$$\{\dot{T}\}_t = (1/\theta\Delta t)(\{T\}_t - \{T\}_{t-\Delta t}) - ((1-\theta)/\theta)\{\dot{T}\}_{t-\Delta t} \qquad (7)$$

Consider equation (5) at time, t, and at an earlier time, t-Δt, to produce the following equations:

$$[S]_t\{T\}_t + [C]\{\dot{T}\}_t = \{R\}_t \qquad (8)$$

$$[S]_{t-\Delta t}\{T\}_{t-\Delta t} + [C]\{\dot{T}\}_{t-\Delta t} = \{R\}_{t-\Delta t} \qquad (9)$$

where the matrix [C] is time invariant.

Substituting equation (7) into equation (8) and rearranging the terms yields the equation:

$$([S]_t+(1/\theta\Delta t)[C])\{T\}_t = ((1-\theta)/\theta)[C]\{\dot{T}\}_{t-\Delta t} + (1/\theta\Delta t)[C]\{T\}_{t-\Delta t} + \{R\}_t \qquad (10)$$

Solving for $\{\dot{T}\}_{t-\Delta t}$ in equation (9) and substituting into equation (10) results in the final equation:

$$([S]_t+1/\theta\Delta t)[C])\{T\}_t = ((1/\theta\Delta t)[C]-((1-\theta)/\theta)[S]_{t-\Delta t})\{T\}_{t-\Delta t} + ((1-\theta)/\theta)\{R\}_{t-\Delta t} + \{R\}_t \qquad (11)$$

Transient temperature distributions are predicted by specifying θ and Δt as well as the normal boundary conditions represented in equation (11). The transient solution is found by an time stepping process, choosing Δt small enough to attain numerical accuracy (see section V). To solve for steady state temperatures by equation (11) would require too many time steps. Alternatively, steady state temperatures are calculated by equation (4).

Equation (11) may now be rewritten in the form:

$$[K]\{T\}_t = \{F\} \qquad (12)$$

The total conductivity matrix, [K], is an NxN non-symmetric banded matrix. N is the total number of nodes in the finite element mesh. The asymmetry of [K] is due to the directional property of the velocity vector which contributes to the term [Kv]. Thus [K] is symmetric only when V = 0. {F} is a single column matrix with N total values forming the right hand side of equation (11). A gaussian elimination technique is used to solve equation (12) for the temperature vector $\{T\}_t$ (N values) at time t, incrementing with steps of Δt.

APPENDIX B

THERMAP FLOWCHART

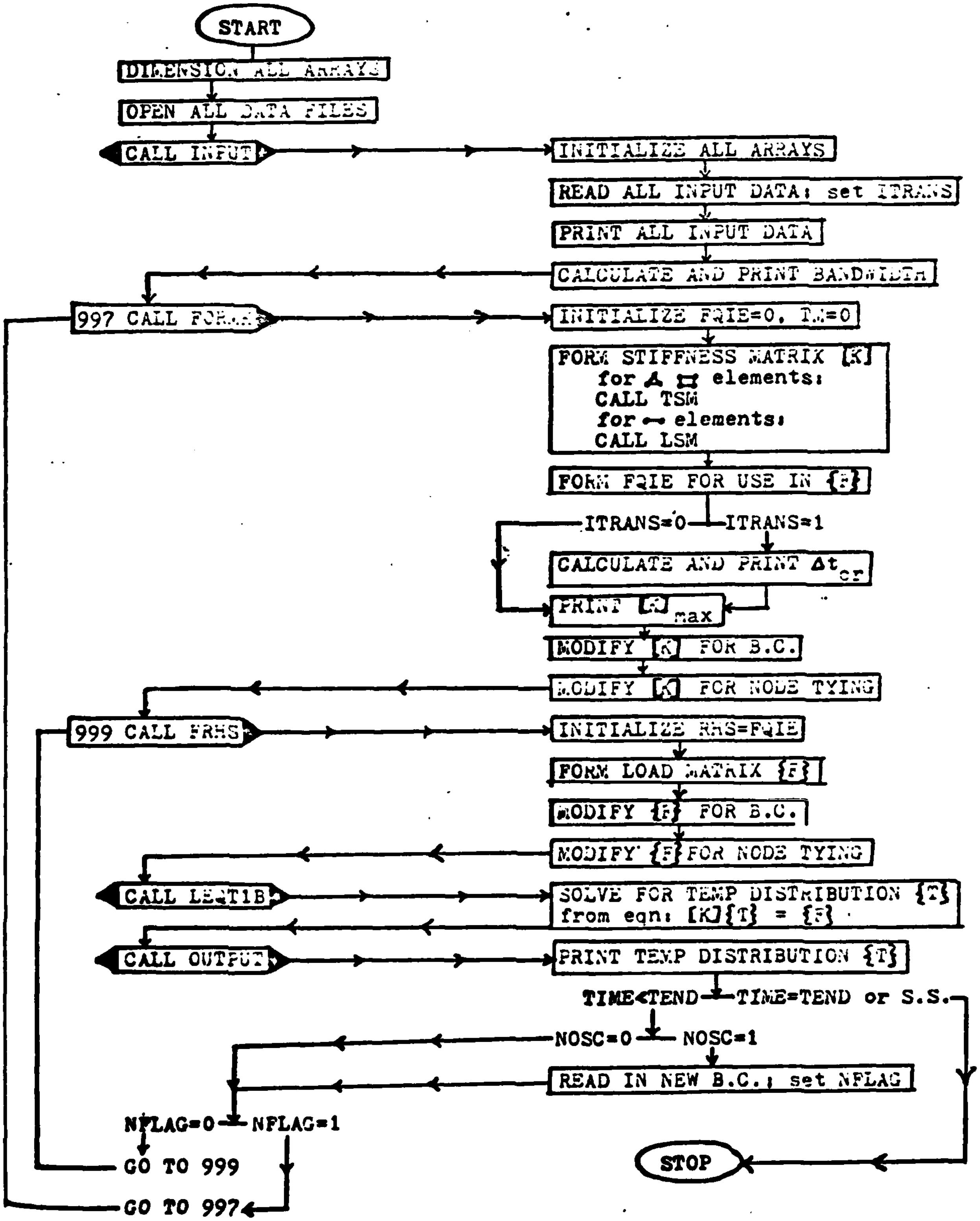
START
DIMENSION ALL ARRAYS
OPEN ALL DATA FILES
CALL INPUT
INITIALIZE ALL ARRAYS
READ ALL INPUT DATA; set ITRANS
PRINT ALL INPUT DATA
CALCULATE AND PRINT BANDWIDTH
997 CALL FORM
INITIALIZE FQIE=0, TM=0
FORM STIFFNESS MATRIX [K]
for ◭ ⌑ elements:
CALL TSM
for ⊷ elements:
CALL LSM
FORM FQIE FOR USE IN {F}
ITRANS=0
ITRANS=1
CALCULATE AND PRINT Δt cr
PRINT [K] max
MODIFY [K] FOR B.C.
MODIFY [K] FOR NODE TYING
999 CALL FRHS
INITIALIZE RHS=FQIE
FORM LOAD MATRIX {F}
MODIFY {F} FOR B.C.
MODIFY {F} FOR NODE TYING
CALL LEQT1B
SOLVE FOR TEMP DISTRIBUTION {T}
from eqn: [K]{T} = {F}
CALL OUTPUT
PRINT TEMP DISTRIBUTION {T}
TIME<TEND
TIME=TEND or S.S.
NOSC=0
NOSC=1
READ IN NEW B.C.; set NFLAG
NFLAG=0
NFLAG=1
GO TO 999
GO TO 997
STOP

APPENDIX C

```
C
C
C
C-------------------THERMAL ANALYSIS PROGRAM----------------------
C
C
C
C MODIFICATIONS LAST MADE ON SEPTEMBER 15,1982 BY F. E. KENNEDY
C
C
C THERMAP SOLVES 2-DIMENSIONAL AND 3-D AXISYMMETRIC HEAT CONDUCTION
C PROBLEMS USING THE FINITE ELEMENT METHOD.
C
C THERMAP ORIGINATED FROM SAMPLE CODE PRESENTED BY K.H. HUEBNER
C IN HIS TEXTBOOK: 'THE FINITE ELEMENT METHOD FOR ENGINEERS'.
C THERMAP'S CAPABILITIES HAVE BEEN EXPANDED, MODIFIED AND UPGRADED
C BY PROFESSOR FRANCIS E. KENNEDY, JR. AND ROGER F. GLOVSKY (M.E. 1982),
C AT THAYER SCHOOL OF ENGINEERING, DARTMOUTH COLLEGE.
C
C THERMAP CAN SOLVE TRANSIENT OR STEADY STATE PROBLEMS FOR THE FOLLOWING
C CONDITIONS: FIXED TEMPERATURE, CONDUCTION, HEAT FLUX NORMAL TO SURFACE
C HEAT FLUX NORMAL TO BOUNDARY, CONVECTION ACROSS SURFACE, CONVECTION
C ALONG BOUNDARY, INTERNAL HEAT GENERATION, AND NODE TYING (EQUATING
C TEMPERATURES AT ANY TWO NODES).  THE HEAT CONDUCTION PROBLEM MAY BE
C 2-D OR 3-D AXISYMMETRIC WITH MOVING OR STATIONARY BODIES.
C THE FINITE ELEMENT MESH MAY CONTAIN QUADRILATERAL,TRIANGULAR,
C OR LINEAR ELEMENTS.  THE MATERIAL PROPERTIES MAY VARY FROM ELEMENT
C  TO ELEMENT, AND MAY BE A FUNCTION OF TEMPERATURE.
C
C THIS FORTRAN PROGRAM REQUIRES ACCESS TO THE FILE PARM.
C  ALL DIMENSIONS FOR ARRAYS ARE SET IN THAT FILE AND ANY CHANGES
C  IN THOSE DIMENSIONS MUST BE MADE IN PARM BEFORE COMPILING AND
C  EXECUTING THERMAP.
C
C INPUT TO THE PROGRAM COMES FROM 14 DATA FILES. THE FILES AND
C THEIR DATA REQUIREMENTS ARE AS FOLLOWS (ALL FILES ARE IN FREE FORMAT):
C
C FILE(7) 'ELFILE' - CONTAINS ELEMENT DATA
C      ONE LINE FOR EACH ELEMENT:
C      [ELEMENT NO., NODE1, NODE2, NODE3, NODE4, MATERIAL NO.]
C      NODES SHOULD BE INPUT COUNTERCLOCKWISE.
C      FOR TRIANGULAR ELEMENTS, SET NODE3 = NODE4.
C      FOR LINEAR ELEMENTS, SET NODE2 = NODE3 = NODE4.
C FILE(8) 'BCFILE' - CONTAINS PRESCRIBED TEMPERATURES
C      ONE LINE FOR EACH PRESCRIBED NODAL TEMPERATURE:
C      [B.C.NUMBER, NODE, PRESCRIBED TEMPERATURE]
C FILE(9) 'IHFILE' - CONTAINS INTERNAL HEAT GENERATION DATA
C      ONE LINE FOR EACH ELEMENT:
C      [CONDITION NUMBER, ELEMENT, QI]
C      QI = HEAT/VOLUME (HEAT SOURCE HAS POSITIVE SIGN)
C FILE(10) 'SHFILE' - CONTAINS PRESCRIBED HEAT FLUX DATA
C      ONE LINE FOR EACH HEAT FLUX BOUNDARY CONDITION.
C      IF HEAT FLUX IS NORMAL TO BOUNDARY SEGMENT, DATA LINE IS:
C      [SEGMENT NO, LEFT NODE, RIGHT NODE, QH]
C      IF HEAT FLUX IS NORMAL TO ELEMENT SURFACE, DATA LINE IS:
C      [SEGMENT NO, ZERO(0), ELEMENT NO, QH]
C      QH = HEAT/AREA  (HEAT SOURCE HAS POSITIVE SIGN)
C FILE(11) 'CBFILE' - CONTAINS PRESCRIBED CONVECTION DATA
C      ONE LINE FOR EACH CONVECTION BOUNDARY CONDITION.
C      IF CONVECTION OCCURS ALONG BOUNDARY SEGMENT, DATA LINE IS:
C      [SEGMENT NO, LEFT NODE, RIGHT NODE, CONVECTION COEFF, AMBIENT TEMP
C      IF CONVECTION OCCURS ACROSS ELEMENT SURFACE, DATA LINE IS:
C      [SEGMENT NO, ZERO(0), ELEMENT NO, CONVECTION COEFF, AMBIENT TEMP]
```

```
C FILE(12) 'QUFILE' - CONTAINS CONTROL INFORMATION
C       LINE 1:  [NN,NE,NBC,NHF,NCB,NHG,NNT,NMA,NTH]
C       LINE 2:  [NCASE,NLIST,NCMP,RATIO,NVEL]
C       LINE 3:  [ITRANS,TBEG,DELT,TEND,MINCR]
C       LINE 4:  [NIT,TINIT,THETA]
C       LINE 5:  [NOSC,MBCINCR,MHFINCR,MVINCR,MCBINCR]
C       LINE 6:  [ITMAX,ERRMAX]
C         NN      = NO. OF NODES
C         NE      = NO. OF ELEMENTS
C         NBC      = NO. OF FIXED TEMPERATURE BOUNDARY CONDITIONS
C         NHF     = NO. OF SEGMENTS WITH PRESCRIBED HEAT FLUX
C         NCB     = NO. OF BOUNDARY SEGMENTS SUBJECT TO CONVECTION
C         NHG     = NO. OF ELEMENTS WITH INTERNAL HEAT GENERATION
C         NNT     = NO. OF NODE TYING PAIRS
C         NMA     = NO. OF DIFFERENT MATERIALS
C         NTH     = NO. OF DIFFERENT THICKNESSES
C         NCASE   = 1 FOR 2-DIMENSIONAL
C                 = 2 FOR AXISYMMETRIC
C         NLIST   = 0 IF ALL INPUT DATA ARE TO BE PRINTED
C                 = 1 IF ONLY BOUNDARY CONDITIONS ARE TO BE PRINTED
C                 = 2 IF NO INPUT DATA ARE TO BE PRINTED
C         NCMP    = 0 FOR NO COMPARISON OF ELEMENT ASPECT RATIOS
C                 = 1 FOR PRINT OUT OF LARGE ELEMENT ASPECT RATIOS
C         RATIO   = MAXIMUM DESIRED ELEMENT ASPECT RATIO (CHOOSE >=0)
C         NVEL    = 0 IF NEITHER BODY IS MOVING
C                 = -1 IF ONE BODY IS TRANSLATING WITH RESPECT TO OTHER
C                 = 1 IF ONE BODY IS ROTATING WITH RESPECT TO OTHER
C         ITRANS = 0  FOR STEADY STATE SOLUTION
C                 = 1  FOR TRANSIENT SOLUTION
C         TBEG    = TIME AT WHICH TRANSIENT SOLUTION WILL BEGIN
C         DELT    = TIME INCREMENT FOR TRANSIENT SOLUTION
C         TEND    = TIME AT WHICH TRANSIENT SOLUTION WILL END
C         MINCR   = NUMBER OF TIME INCREMENTS DESIRED BETWEEN PRINTOUTS
C         NIT     = 1 FOR READING INITIAL TEMPS FROM FILE(15)
C                 = 0 FOR UNIFORM INITIAL TEMPS
C         TINIT   = INITIAL TEMPERATURE (UNIFORM)
C         THETA   = WEIGHT FUNCTION FOR NEWMARK RECURSION RELATION
C         NOSC    = 1 FOR CHANGING BOUNDARY CONDITIONS
C                   0 FOR CONSTANT BOUNDARY CONDITIONS
C         MBCINCR= NO OF TIME INCREMENTS BETWEEN CHANGING FIXED B.C.
C         MHFINCR= NO OF TIME INCREMENTS BETWEEN CHANGING H.F. CONDITIONS
C         MVINCR = NO OF TIME INCREMENTS BETWEEN CHANGING VELOCITY CONDITIONS
C         MCBINCR= NO OF TIME INCREMENTS BETWEEN CHANGING CONVECT. CONDITIONS
C         ITMAX=MAX NO OF TEMPERATURE SOLUTIONS TO ACHIEVE PROPERTY
C                CONVERGENCE
C         ERRMAX=MAX ALLOWABLE ERROR IN MATERIAL PROPERTIES
C FILE(13) 'MAFILE' - CONTAINS MATERIAL PROPERTY DATA
C       ONE SET OF LINES FOR EACH DIFFERENT MATERIAL
C        FIRST LINE IN SET:  [MAT,IMAT,NUMTC]
C         MAT=MATERIAL NUMBER (REFERENCED IN ELEMENT FILE)
C         IMAT= 1 FOR MATERIAL IN BODY MOVING RELATIVE TO HEAT SOURCE
C               0 FOR BODY STATIONARY RELATIVE TO HEAT SOURCE
C         NUMTC=NO OF TEMPERATURES AT WHICH PROPERTIES GIVEN (MAX=8)
C        REMAINING LINES IN SET (NUMTC MORE LINES)
C         TEMPERATURE,X-CONDUCTIVITY,Y-CONDUCTIVITY,DENSITY,SPECIFIC HEAT
C FILE(14) 'TDFILE' - CONTAINS THICKNESS DATA
C       MULTIPLE LINES FOR EACH DIFFERENT THICKNESS:
C       [THICKNESS, NO OF ELEMENTS WITH THAT THICKNESS]
C       [LIST OF ELEMENTS WITH THAT THICKNESS]
C FILE(15) 'TEFILE' - CONTAINS RESULTING TEMPERATURE DISTRIBUTION
C       [TEMP, TEMP, TEMP, TEMP, TEMP, TEMP, TEMP]
C FILE(16) 'RHFILE' - CONTAINS OLD RIGHT HAND SIDE MATRIX
C       [RHSO, RHSO, RHSO, RHSO, RHSO, RHSO, RHSO]
C FILE(17) 'VEFILE' - CONTAINS VELOCITY OF MOVING BODY
C       [OMEGA,XROT,YROT]
C         OMEGA   = ANGULAR VELOCITY IF BODY IS ROTATING
C                 = ZERO IF BODY IS TRANSLATING
C         XROT    = X COORDINATE OF CENTER OF ROTATING BODY
C                   X COMPONENT OF VELOCITY IF TRANSLATING
C         YROT    = Y COORDINATE OF CENTER OF ROTATING BODY
C                   Y COMPONENT OF VELOCITY IF TRANSLATING
C FILE(18) 'NTFILE' - CONTAINS NODE TYING DATA
C       [BC NO., NODE, NODE]
C FILE(19) 'NOFILE' - CONTAINS NODAL POINT COORDINATES
C       ONE LINE FOR EACH NODE:
C       [NODE NUMBER, X(OR R) COORD, Y(OR Z) COORD]
C FILE(29) 'NFILE' -CONTAINS NAMES OF ALL DATA FILES
C      ONE LINE FOR EACH FILE NAME,FROM FILE(7) TO FILE(19):
C       ['FILENAME']
C
```

Appendix C (continued)

```
C****************************** SAMPLE MESH **********************************
C
C               Y
C               !       BC       BC
C               !       75       75
C         SH   (1)------(4)------(7)-----(10)-----(13)-----(16)  CB
C          75~~)!        !        !       !        !        !(~~50
C          75~~)!   #1   !   #3   !  #5   !   #7   !   #9   !(~~50
C          75~~)!        !        !                !        !(~~50
C              (2)------(5)------(8)-----(11)-----(14)-----(17)
C          75~~)!        !        !       !        !        !(~~50
C          75~~)!   #2   !   #4   !  #6   !   #8   !  #10   !(~~50
C          75~~)!        !        !       !        !        !(~~50
C              (3)------(6)------(9)-----(12)-----(15)-----(18)----X
C                       25       25
C                       BC       BC
C
C
C****************************** SAMPLE FILES *********************************
C
C     NFILE               NOTEST                 ELTEST           BCTEST
C     ------              ------                 ------           ------
C                         1,0,.1               1,1,2,5,4,3          1,4,75
C    'ELTEST'             2,0,.05              2,2,3,6,5,3          2,7,75
C    'BCTEST'             3,0,0                3,4,5,8,7,3          3,6,25
C    'IHTEST'             4,.05,.1             4,5,6,9,8,3          4,9,25
C    'SHTEST'             5,.05,.05            5,7,8,11,10,3
C    'CBTEST'             6,.05,0              6,8,9,12,11,3
C    'QUTEST'             7,.1,.1              7,10,11,14,13,6
C    'MATEST'             8,.1,.05             8,11,12,15,14,6
C    'TDTEST'             9,.1,0               9,13,14,17,16,6
C    'TETEST'            10,.15,.1            10,14,15,18,17,6
C    'RHTEST'            11,.15,.05
C    'VETEST'            12,.15,0
C    'NTTEST'            13,.2,.1
C    'NOTEST'            14,.2,.05
C                        15,.2,0
C                        16,.25,.1
C                        17,.25,.05
C                        18,.25,0
C
C     QUTEST                 CBTEST                 MATEST             VETEST
C     ------                 ------                 ------             ------
C 18,10,4,3,2,2,3,2,1      1,16,17,38,50          3,0,1                0,0,100
C 1,0,1,2.5,-1             2,17,18,38,50          100,600,600,20,20
C 1,0.,.0001,.002,10                              6,1,2
C 0,5,.5005                                       0,300,300,30,5
C 1,5,5,5,5                                      200,500,400,32,10
C 10,5
C
C SHTEST         IHTEST            TDTEST             NTTEST
C ------         ------            ------             ------
C 1,1,2,75       1,9,1000          1.25,10            1,1,16
C 2,2,3,75       2,10,1000         1,2,3,4,5          2,2,17
C                                  6,7,8,9,10         3,3,18
C******************************************************************************
```

APPENDIX D

LIST OF PUBLICATIONS AND PRESENTATIONS RESULTING FROM THIS RESEARCH

Publications

1. Kennedy, F.E. and Karpe, S.A., "Thermocracking of a Mechanical Face Seal", Wear, 79 (1982), pp. 21-36.
2. Kennedy, F.E. and Grim, J.N., "Observation of Contact Conditions in Mechanical Face Seals", to be published by ASLE.

Reports and Theses

1. Kennedy, F.E., Grim, J.N., and Glovsky, R.P., "Factors Influencing Thermomechanical Failure of Face Seals", Interim Report #1 submitted to ONR, Thayer School of Engineering, January 1982.
2. Glovsky, R.P., "Development and Application of THERMAP", Master of Engineering Thesis, Thayer School of Engineering, June 1982.
3. Grim, J.N., "Observation of Thermoelastic Instabilities in Mechanical Face Seals", Master of Engineering Thesis, Thayer School of Engineering, July 1982.

Other Presentations

1. Kennedy, F.E., "Thermomechanical Failure of a Mechanical Face Seal", presented at Navy/NASA Seals Workshop, Albuquerque, N.M., October 1981.

APPENDIX E

DISTRIBUTION LIST - TRIBOLOGY

One copy except
as noted

Mr. M. Keith Ellingsworth 2
Engineering Sciences Directorate
Office of Naval Research
800 N. Quincy Street
Arlington, VA 22217

Defense Documentation Center 12
Building 5, Cameron Station
Alexandria, VA 22314

Technical Information Division 6
Naval Research Laboratory
4555 Overlook Avenue SW
Washington, DC 20375

Division of Weapons & Engineering
U. S. Naval Academy
Annapolis, MD 21402

D. L. Bonner, LMM
Headquarters, U. S. Marine Corps
Washington, DC 20380

Colonel R. Bowles, USMC
Marine Corps Liaison Officer
Office of Naval Research
800 N. Quincy Street
Arlington, VA 22217

Mr. R. G. Brown
Code 2382
DTNSRDC
Annapolis, MD 21402

Dr. J. Dell POSL 1
Air Force Wright Aeronautical Laboratories
Wright- Patterson Air Force Base
Dayton, OH 45433

M. J. Devine
General Technology
2560 Prescott Road
Havertown, PA 19083

A. J. D'Orazio, Code PE-72
Naval Air Propulsion Center
Trenton, NJ 08628

Mr. Jim Dray
Head, Friction & Wear Branch
DTNSRDC
Annapolis, MD 21402

F. C. Gale
NAVMAT
Code OOKB, CP5, Room 606
Washington, DC 20360

Mr. Richard R. Graham, II
Code 5243, Bldg. NC4
Naval Sea Systems Command
Washington, DC 20362

Mr. Al Harbage, Jr.
Code 2723
DTNSRDC
Annapolis, MD 21402

Mr. Martin Kandl
Code 5231
Naval Sea Systems Command
Washington, DC 20362

S. Karpe
David W. Taylor Naval Ship R & D Center
Ship Materials Engineering Department
Annapolis, MD 21402

Dr. R. N. Katz
Army Materials and Mechanics Research Center
Watertown, MA 02172

Lt. Col. R. Kerr, USMC
Mobility and Logistics Division
Development Center
MCDEC
Quantico, VA 22134

L. Kociuba, Code 92A3
Naval Air Engineering Center
Lakehurst, NJ 08733

A. J. Koury - AIR-4111D
Naval Air Systems Command
Washington, DC 20361

Dr. George Mayer
Director, Metallurgy and
Materials Science Division
Army Research Office
P. O. Box 12211
Research Triangle Park, NC 27709

B. D. McConnell - MLBT
Air Force Wright Aeronautical Laboratories
Wright-Patterson Air Force Base
Dayton, OH 45433

W. McGovern
U. S. Army MERDC
Fort Belvoir, VA 22060

D. V. Minuti
Code 606B
Naval Air Development Center
Warminster, PA 18974

Dr. Jim D. Murday
Code 6170
Naval Research Laboratory
Washington, DC 20375

Mr. Cliff Mussen
PMS 396-223
Naval Sea Systems Command
Washington, DC 20362

Mr. A. B. Neild, Jr.
Head, Power Transmission Branch
DTNSRDC
Annapolis MD 21402

NASA-Lewis Research Center
Attn: Mr. Jim Kiraly
21000 Brookpark Road
Cleveland, OH 44135

J. W. Patten
Battelle Memorial Institute Pacific
Northwest Laboratories
Richland, WA 99352

Dr. Earl Quandt, Jr.
Head, Power Systems Division
DTNSRDC
Annapolis, MD 21402

Dr. A. W. Ruff
Metal Science and Standards Division
National Bureau of Standards
Washington, DC 20234

Mr. Ken R. Sasdelli
Code 2723
DTNSRDC
Annapolis, MD 21402

R. Schmidt, AIR-320
Naval Air Systems Command
Washington, DC 20361

Dr. R. Schumaker, AIR-340
Naval Air Systems Command
Washington, DC 20361

David S. Siegel
Code 260
Office of Naval Research
800 N. Quincy Street
Arlington, VA 22217

L. Stallings,
Code 6061
Naval Air Development Center
Warminster, PA 18974

Mr. Richard Strucko
Code 2723
DTNSRDC
Annapolis, MD 21402

Dr. N. P. Suh
Massachusetts Institute of Technology
Department of Mechanical Engineering
Cambridge, MA 02139

Dr. Fred J. Tribe
Admiralty Marine Technology Establishment
Holten Heath, Poole, Dorset
U.K. BH166JU

Dr. E. Van Reuth
Defense Advanced Research Project Agency
1400 Wilson Blvd.
Arlington, VA 22209

Dr. Frank Ventriglio
Code 05R14
Naval Sea Systems Command
Washington, DC 20362

P. Wienberg, AIR-5304C
Naval Air Systems Command
Washington, DC 20361

Dr. R. D. Arnell
Department of Aeronautical &
Mechanical Engineering
University of Salford
Salford, U.K. M54WT

Professor Ralph A. Burton
Chairman, Mechanical and Aerospace Engineering Department
North Carolina State University
3211 Broughton Hall
Raleigh, NC 27650

Professor N. S. Eiss, Jr.
Department of Mechanical Engineering
Virginia Polytechnic Institute
and State University
Blacksburg, VA 24061

Professor I. Etsion
Department of Mechanical Engineering
Technion, Haifa
Israel

Professor Hasselman
Virginia Polytechnic Institute
Department of Materials Engineering
Blacksburg, VA 24061

Professor William F. Hughes
Mechanical Engineering Dept.
Carnegie Mellon University
Pittsburgh, PA 15213

Professor Frederick D. Ju
Bureau of Engineering Research
University of New Mexico
Albuquerque, NM 87131

Professor T. Keith
Department of Mechanical Engineering
University of Toledo
Toledo, OH 43606

Professor Francis E. Kennedy, Jr.
Thayer School of Engineering
Darthmouth College
Hanover, NH 03755

Professor Alan O. Lebeck
Bureau of Engineering Research
University of New Mexico
Albuquerque, NM 87131

Professor Fred F. Ling
Department of Mechanics
Rensselaer Polytechnic Institute
Troy, NY 12131

Professor K. Ludema
Department of Mechanical Engineering
University of Michigan
Ann Arbor, MI 48105

Professor W. Kenneth Stair
Associate Dean for Research
University of Tennessee
Knoxville, TN 37916

Dr. H. Wilsdorf
Department of Materials
University of Virginia
Charlottesville, VA 22901

Batelle Columbus Laboratories
  Attn: Dr. Richard Jentgen
505 King Avenue
Columbus, OH 43201

BHRA Fluid Engineering
  Attn: Dr. Bernard S. Nau
Cranfield, Bedford
England MK430AJ

Franklin Research Center
  Attn: Mr. Harry Ripple
Twentieth & Parkway
Philadelphia, PA 19103

Wear Sciences
  Attn: Mr. Marshall Peterson
925 Mallard Circle
Arnold, MD 21012

Westinghouse R&D Center
  Attn: Dr. Ian McNab
1310 Beulah Road
Pittsburgh, PA 15235

Mr. Edward L. Wiehe
TRW, Inc.
1 Space Park
Redondo Beach, CA 90278

END

FILMED

3-83

DTIC